IEEE Access
Multidisciplinary | Rapid Review | Open Access Journal

Date of publication xxxx 00, 0000, date of current version xxxx 00, 0000.

Digital Object Identifier 10.1109/ACCESS.2017.DOI

Distributed Robust Formation Control of Heterogeneous Multi-UAVs with Disturbance Rejection

IMIL HAMDA IMRAN[1], DILEK FUNDA KURTULUS[2,3], AZHAR M. MEMON[1], SRIKANTH GOLI[1], TAIBA KOUSER[1], LUAI MUHAMMAD ALHEMS[1].

[1]Applied Research Center for Metrology, Standards, and Testing (ARC-MST), King Fahd University of Petroleum and Minerals, Saudi Arabia
[2]Aerospace Engineering, Middle East Technical University, 06800, Turkey
[3]EKOFLY Engineering Company, (METU Technopolis), Ankara, 06800, Turkey

Corresponding authors: Imil Hamda Imran, Srikanth Goli (e-mail: imil.imran@kfupm.edu.sa, srikanth.goli@kfupm.edu.sa).

ABSTRACT This paper investigates the formation control of multiple heterogeneous quadrotor unmanned aerial vehicles (UAVs). The research focuses on developing a distributed robust formation control strategy to effectively manage the translational and attitude motions of the UAVs utilizing an active virtual leader. The communication of each agent in a connected environment is represented by a directed graph. To align with real applications, only a minimum of one agent is required to connect with the leader. The challenge associated with controlling systems is more complicated by the inherent heterogeneity of UAVs, characterized by variations in their model parameters and the presence of external disturbances in the system dynamics. A robust term is proposed to handle time-varying disturbances added to the closed-loop systems. A comprehensive mathematical proof and numerical illustrations are provided to validate the efficacy of the proposed formation control strategy.

INDEX TERMS quadrotor, unmanned aerial vehicles, distributed robust control, formation control, external disturbances.

I. INTRODUCTION

THE advent of cyber-physical systems represents a novel paradigm, driven by the rapid progress of cutting-edge technologies within the fields of industrial autonomous systems. A key focus within this domain, driving significant technological advancements, is the facilitation of autonomous operation and cognitive capabilities in a networked setting for a collaborative ensemble of multiple quadrotors [1]–[3]. Diverse conditions have yielded numerous insightful findings, yet the overarching goal persists in formulating robust control systems for cooperative Unmanned Aerial Vehicles (UAVs) navigating real-world environments.

Quadrotors find extensive utility across various applications, particularly in hazardous contexts where human intervention proves challenging. These utilizations encompass tasks such as the decommissioning of nuclear facilities, the capture of geospatial imagery, monitoring volcanic activities, and the implementation of precise techniques in agriculture [4], [5].

1) Literature Review and Motivation

One crucial aspect of control design lies in addressing nonlinearities within both translational and attitude dynamics. A conventional approach involves employing a linear controller tailored to a linearized dynamic model, which is applicable only in specific scenarios. Alternative methods such as linear quadratic (LQ) and proportional-integral-derivative (PID) control were developed to address tracking control problems in UAVs, as discussed in [6]–[10]. To handle the complete nonlinear operational spectrum of UAVs, the adoption of a nonlinear controller featuring feedback linearization becomes imperative, as highlighted in [11]. Due to the existence of nonlinear dynamic uncertainties and external disturbances in UAVs, the need for advanced control strategies becomes apparent.

Robust control and adaptive control emerge as two prevalent strategies for managing nonlinear functions fraught with parametric uncertainties. Robust control handles the unknown nonlinear terms by dominating them with some robust terms to maintain the closed-loop system. A case in this point can be found in [12]–[14], where a robust nonlinear

sliding mode control (SMC) technique was utilized to tackle the trajectory tracking difficulties associated with the attitude dynamics of an individual UAV, particularly to handle disturbances and unknown parameters. Further interesting applications of robust control were investigated in [15]–[18].

Meanwhile, adaptive control techniques were employed to handle nonlinear dynamics with uncertain parameters and the presence of external disturbances. Pertinent works in this domain to deal with unknown constant parameters can be found in [19], [20]. Model-free adaptive SMC was developed for tilt trirotor in [21]. Extended model reference adaptive control (MRAC) was studied in [22] for UAVs to handle unknown inertia parameters. Other applications of adaptive schemes for UAVs were developed in [23], [24].

Similar to the individual setting, the presence of parametric uncertainties and unknown disturbances also cause significant challenges in formulating effective control protocols in a collaborative setting. To address these challenges, both robust and adaptive control methodologies are also frequently employed. Some studies using robust control approaches were proposed in [25], [26]. Meanwhile, investigations into adaptive control techniques for collaborative settings have yielded interesting outcomes, as studied in [27].

There are two distinct lines of control strategies employed in collaborative control as discussed in [28]. The first approach is centralized control, where a central unit formulates control input for every agent utilizing the comprehensive global information available within the network. However, this method incurs higher implementation costs. The second strategy is distributed or decentralized control, where each agent autonomously generates its controller without relying on global network information. In this scenario, local control protocols are devised by individual agents based on information received from connected neighbors. Distributed control is considered more practical for real-world settings, especially when dealing with resource-constrained agents. Nevertheless, designing such controllers poses a greater challenge, particularly in systems characterized by uncertainties. Additionally, in cases where the system operates within a directed network, the Laplacian matrix becomes asymmetric, introducing significant complexity to the problem at hand.

Linearizing the system dynamics of each UAV in a networked environment is also one method proposed to maintain the cooperative control of multi-UAVs. The idea is to simplify the control problem in the closed loop systems, hence a linear cooperative control strategy can be extended to maintain the agent. One study for a consensus control for multi-UAVs in this approach can be found in [29], [30]. Several control strategies were investigated by simplifying the nonlinear dynamics [31]–[33]. Also, these approaches avoided the complexities associated with designing controllers in the presence of external disturbances. A robust control scheme was introduced in [34] to deal with nonlinear dynamics, even in the absence of external disturbances. This approach was evaluated through experimental tests, validating its efficacy and applicability in practical settings.

Leader-follower formation control for multi-UAVs was developed in [35] without linearizing the nonlinear dynamics. However, the challenging parts of cooperative control problems were avoided, where all followers connected to the leader. Moreover, the control problem is simplified by the absence of external disturbances in the closed-loop systems. More advanced control approaches were developed in [36]–[38]. The nonlinear terms of the dynamical model are considered in the proposed design. However, the influence of external disturbances was not taken into consideration.

SMC was extended for leader-follower consensus control in [39] without disturbances. However, this approach is applicable in a decentralized fashion only within specific scenarios, where the control input values of connected neighbors are essential for generating the local control input of each agent. In [40], distributed nonlinear formation control was developed for multiple UAVs without disturbances under switching topology. Nonlinear cooperative control of multi-UAVs was explored nonlinear cooperative control for multi-UAV systems without external disturbances employing extended observer and neural networks in [41] and using integrated backstepping control and finite-time control in [42].

A more complicated scenario focused on devising a distributed control scheme capable of managing uncertain parameters in the absence of external disturbances was investigated in [43]. Recently, a predefined time formation control protocol was developed to handle unknown disturbances in [44]. Another robust scheme for tracking control of UAVs was explored in [45]. The tracking formation control was effectively achieved by each agent. However, the simulation results revealed the presence of steady-state chattering in control inputs. This phenomenon is a common occurrence in robust control designs dealing with external disturbances. From the above review, designing a distributed controller for multiple nonlinear UAVs in the presence of external disturbances escalates the complexity of the control problem. Developing a suitable control protocol is essential to effectively tackle this issue.

2) Contribution and Paper Structure

This paper presents a distributed robust strategy aimed at achieving leader-follower formation consensus among multiple UAVs within a directed network. The contribution of this work lies in its ability to address the diverse characteristics inherent in each UAV, caused by various parameters of the dynamical model. In real-world applications, UAVs often possess unique physical properties, such as different sizes, weights, and propulsion systems, leading to variations in their dynamics. Managing these differences is crucial for effective collaboration and coordination among UAVs, particularly in formation flight scenarios where precise control is essential. To this end, the proposed control mechanism is designed to accommodate the inherent diversity of multi-UAV systems, ensuring robust performance across a range of operating conditions.

Moreover, the proposed design demonstrates robustness

against unknown time-varying external disturbances affecting both translational and rotational dynamics. In practical UAV missions, environmental factors such as wind gusts, and turbulence can introduce disturbances that affect the stability and performance of the control system. Addressing these disturbances is critical for achieving reliable and accurate formation control. The proposed control protocol employs robust control techniques to mitigate the effects of such disturbances, thus enhancing the overall robustness and effectiveness of the multi-UAV system.

It is important to note that the control architecture operates without reliance on global state information, leveraging specific individuals or designated agents with access to the leader and connected neighbors. In large-scale UAV networks, obtaining and maintaining global state information can be challenging due to communication constraints, being expensive in applications, and limited computational resources. By decentralizing the control scheme, the suggested approach offers flexibility and adaptability to dynamic environments.

An extended approach is employed to reduce the chattering issue often encountered in conventional SMC, achieved by approximating the non-smooth function with a robust representation, thus attenuating chattering within the proposed controller. Chattering, characterized by non-smooth control inputs, can lead to mechanical wear and instability in UAV systems, compromising performance and safety. The proposed method improves upon conventional SMC techniques by introducing a smoother function while preserving the robustness properties inherent in SMC.

The contribution of this scheme is further emphasized within the context of a directed graph network, where the associated Laplacian matrix lacks symmetry. This asymmetry elevates the complexity involved in designing distributed controllers, necessitating more generalized communication between each agent and the leader. In practical UAV networks, communication links may exhibit asymmetric characteristics due to varying signal strengths and network topology. The suggested approach accounts for these asymmetries in communication channels, ensuring effective information exchange and coordination among multi-UAVs within the network.

These contributions collectively highlight the robust and distributed nature of the control strategy, demonstrating its applicability and effectiveness in the formation control of multi-UAVs. By addressing the challenges of heterogeneous dynamics, unknown disturbances, and asymmetric communication networks, the proposed control protocol offers a solution for achieving reliable and precise formation control among heterogeneous multiple UAVs.

The subsequent sections of this paper are structured as follows. Section II introduces the dynamical model of UAVs. Subsequently, Section III presents the proposed tracking control design, accompanied by a stability analysis encompassing both the outer and inner loop of the UAVs. In Section IV, the efficacy of the proposed design is evaluated through the presentation of numerical analyses and simulation results. Finally, Section V summarizes the paper and offers brief recommendations for future research directions.

II. SYSTEM DYNAMICS OF MULTIPLE UAVS

A. TRANSLATIONAL DYNAMICS

Consider the translational dynamics of the i-th UAV or agent i represented by

$$\ddot{\eta}_{p_i} = (-g + \delta_{z_i})z_e + J_{t_i} z_e \frac{u_{t_i}}{m_i}, \tag{1}$$

or

$$\ddot{x}_i = w_{x_i} \frac{u_{t_i}}{m_i} \tag{2}$$

$$\ddot{y}_i = w_{y_i} \frac{u_{t_i}}{m_i} \tag{3}$$

$$\ddot{z}_i = -g + \delta_{z_i} + w_{z_i} \frac{u_{t_i}}{m_i} \tag{4}$$

where

$$\eta_{p_i} = \begin{bmatrix} x_i & y_i & z_i \end{bmatrix}^\intercal$$

$$z_e = \begin{bmatrix} 0 & 0 & 1 \end{bmatrix}^\intercal$$

$$J_{t_i} = \begin{bmatrix} \cos\theta_i \cos\psi_i & \sin\phi_i \sin\theta_i \cos\psi_i - \cos\phi_i \sin\psi_i & \cos\phi_i \sin\theta_i \cos\psi_i + \sin\phi_i \sin\psi_i \\ \cos\theta_i \sin\psi_i & \sin\phi_i \sin\theta_i \sin\psi_i + \cos\phi_i \cos\psi_i & \cos\phi_i \sin\theta_i \sin\psi_i - \sin\phi_i \cos\psi_i \\ -\sin\theta_i & \sin\phi_i \cos\theta_i & \cos\phi_i \cos\theta_i \end{bmatrix}$$

$$w_{x_i} = \cos\phi_i \sin\theta_i \cos\psi_i + \sin\phi_i \sin\psi_i$$

$$w_{y_i} = \cos\phi_i \sin\theta_i \sin\psi_i - \sin\phi_i \cos\psi_i$$

$$w_{z_i} = \cos\phi_i \cos\theta_i.$$

The translational position of UAV i represents by $x_i \in \mathbb{R}$, $y_i \in \mathbb{R}$, and $z_i \in \mathbb{R}$. The mass of agent i and gravitational acceleration are denoted by $m_i \in \mathbb{R}$ and $g \in \mathbb{R}$, respectively. Note that the values of ϕ_i and θ_i are in between $-\frac{\pi}{2}$ to $\frac{\pi}{2}$, thus $\cos\phi_i \neq 0$ and $\cos\theta_i \neq 0$, Therefore, $J_{t_i}^\intercal = J_{t_i}^{-1}$.

The external disturbance is denoted by $\delta_{z_i}(t) \in \mathbb{R}$ satisfying Assumption 1.

Assumption 1: The translational dynamics of the UAV experience external disturbances such that $|\delta_{z_i}(t)| \leq d_{z_i}$, where d_{z_i} is a constant.

The disturbance $\delta_z(t)$ is unknown for feedback control design. Hence, addressing uncertainties using the full feedback linearization method is not a straightforward application.

A graph $\mathcal{G} = \{\mathcal{V}, \mathcal{E}\}$ represents the network topology, where $\mathcal{V} = \{1, 2, \cdots, n\}$ is a finite non-empty set of nodes and $\mathcal{E} \subset \mathcal{V} \times \mathcal{V}$ is the set of directed edges. Matrix $\mathcal{A} = [a_{ij}]$ represents adjacency matrix such that $a_{ij} > 0$ if the edge $(j, i) \in \mathcal{E}$, $i \neq j$. The weight in-degree of node i as i-th row sum of $\mathcal{A}$ is denoted by D, where $d_i = \sum_{j=1, i\neq j}^{n} a_{ij}$ and $D = \text{diag}\left(\begin{bmatrix} d_1 & \cdots & d_n \end{bmatrix}\right) \in \mathbb{R}^{n\times n}$. The Laplacian matrix representing the communication network is denoted by L, where $L = D - \mathcal{A}$. The communication between the leader and followers is represented by $B = \text{diag}\left(\begin{bmatrix} b_1 & \cdots & b_n \end{bmatrix}\right)$, where $b_i \geq 0$ the weight from agent i to the leader.

The translational dynamics (2),(3), and (4) can be written in compact form as follows

$$\ddot{x} = w_x m^{-1} u_t \tag{5}$$
$$\ddot{y} = w_y m^{-1} u_t \tag{6}$$
$$\ddot{z} = -\mathbf{1}_n g + \delta_z + w_z m^{-1} u_t \tag{7}$$

where

$$\begin{aligned}
x &= \begin{bmatrix} x_1 & \cdots & x_n \end{bmatrix}^\intercal \in \mathbb{R}^n \\
y &= \begin{bmatrix} y_1 & \cdots & y_n \end{bmatrix}^\intercal \in \mathbb{R}^n \\
z &= \begin{bmatrix} z_1 & \cdots & z_n \end{bmatrix}^\intercal \in \mathbb{R}^n \\
w_x &= \text{diag}\left(\begin{bmatrix} w_{x_1} & \cdots & w_{x_n} \end{bmatrix}\right) \in \mathbb{R}^{n\times n} \\
w_y &= \text{diag}\left(\begin{bmatrix} w_{y_1} & \cdots & w_{y_n} \end{bmatrix}\right) \in \mathbb{R}^{n\times n} \\
w_z &= \text{diag}\left(\begin{bmatrix} w_{z_1} & \cdots & w_{z_n} \end{bmatrix}\right) \in \mathbb{R}^{n\times n} \\
m &= \text{diag}\left(\begin{bmatrix} m_1 & \cdots & m_n \end{bmatrix}\right) \in \mathbb{R}^{n\times n} \\
u_t &= \begin{bmatrix} u_{t_1} & \cdots & u_{t_n} \end{bmatrix}^\intercal \in \mathbb{R}^n \\
\delta_z &= \begin{bmatrix} \delta_{z_1} & \cdots & \delta_{z_n} \end{bmatrix}^\intercal \in \mathbb{R}^n \\
\mathbf{1}_n &= \begin{bmatrix} 1 & \cdots & 1 \end{bmatrix}^\intercal \in \mathbb{R}^n
\end{aligned}$$

There exists a virtual leader connected at least to one follower. Its translational states are represented by $x_0 \in \mathbb{R}$, $y_0 \in \mathbb{R}$, and $z_0 \in \mathbb{R}$. This virtual leader has some constraints stated in the following assumption.

Assumption 2: The dynamics of a virtual leader is bounded such that $\|\ddot{x}_0\| \leq x_m$, $\|\ddot{y}_0\| \leq y_m$, and $\|\ddot{z}_0\| \leq z_m$, where x_m, y_m, and z_m are some known constants.

B. ATTITUDE DYNAMICS

The attitude dynamics of the i-th UAV (agent i) are represented by

$$\ddot{\phi}_i = w^1_{\phi_i} f_{\phi_i} + w^2_{\phi_i} \tau_{\phi_i} + \delta_{\phi_i} \tag{8}$$
$$\ddot{\theta}_i = w^1_{\theta_i} f_{\theta_i} + w^2_{\theta_i} \tau_{\theta_i} + \delta_{\theta_i} \tag{9}$$
$$\ddot{\psi}_i = w^1_{\psi_i} f_{\psi_i} + w^2_{\psi_i} \tau_{\psi_i} + \delta_{\psi_i} \tag{10}$$

where

$$\begin{aligned}
w^1_{\phi_i} &= \frac{I_{y_i} - I_{z_i}}{I_{x_i}},\ f_{\phi_i} = \dot{\theta}_i \dot{\psi}_i,\ w^2_{\psi_i} = \frac{1}{I_{x_i}} \\
w^1_{\theta_i} &= \frac{I_{z_i} - I_{x_i}}{I_{y_i}},\ f_{\theta_i} = \dot{\phi}_i \dot{\psi}_i,\ w^2_{\psi_i} = \frac{1}{I_{y_i}} \\
w^1_{\psi_i} &= \frac{I_{x_i} - I_{y_i}}{I_{z_i}},\ f_{\psi_i} = \dot{\phi}_i \dot{\theta}_i,\ w^2_{\psi_i} = \frac{1}{I_{z_i}}.
\end{aligned}$$

The orientation angles of UAV i composed of roll, pitch, and yaw are represented by $\phi_i \in \mathbb{R}$, $\theta_i \in \mathbb{R}$, and $\psi_i \in \mathbb{R}$, respectively. The torques acting on the body frame of attitude dynamics are denoted by $\tau_{\phi_i} \in \mathbb{R}$, $\tau_{\theta_i} \in \mathbb{R}$, and $\tau_{\psi_i} \in \mathbb{R}$. The inertia parameters of agent i are represented by I_{x_i}, I_{y_i}, and I_{z_i}. The inertia parameters can differ for each UAV, indicating that the multiple UAV system examined in this paper belongs to the category of heterogeneous multi-agent systems (MASs).

An external disturbance is added to every attitude state of agent i denoted by $\delta_{\phi_i} \in \mathbb{R}$, $\delta_{\theta_i} \in \mathbb{R}$, and $\delta_{\psi_i} \in \mathbb{R}$ to represent practical setting. These external disturbances satisfy the following assumption.

Assumption 3: The external disturbances influencing rotational dynamics satisfy the following inequalities

$$\|\delta_{\phi_i}\| \leq d_{\phi_i},\ \|\delta_{\theta_i}\| \leq d_{\theta_i},\ \|\delta_{\psi_i}\| \leq d_{\psi_i} \tag{11}$$

where d_{ϕ_i}, d_{θ_i} and d_{ψ_i} are some constants.

Similar to translational dynamics, δ_{ϕ_i}, δ_{θ_i}, and δ_{ψ_i} are not available for the feedback control design. Hence, a full feedback linearization method cannot be straightforwardly applied to maintain multi-UAV motion.

The attitude dynamics (8), (9), and (10) can be written in compact forms

$$\begin{aligned}
\ddot{\phi} &= w^1_{\phi} f_{\phi} + w^2_{\phi} \tau_{\phi} + \delta_{\phi} \\
\ddot{\theta} &= w^1_{\theta} f_{\theta} + w^2_{\theta} \tau_{\theta} + \delta_{\theta} \\
\ddot{\psi} &= w^1_{\psi} f_{\psi} + w^2_{\psi} \tau_{\psi} + \delta_{\psi}
\end{aligned} \tag{12}$$

where

$$\begin{aligned}
\phi &= \begin{bmatrix} \phi_1 & \cdots & \phi_n \end{bmatrix}^\intercal \in \mathbb{R}^n \\
\theta &= \begin{bmatrix} \theta_1 & \cdots & \theta_n \end{bmatrix}^\intercal \in \mathbb{R}^n \\
\psi &= \begin{bmatrix} \psi_1 & \cdots & \psi_n \end{bmatrix}^\intercal \in \mathbb{R}^n \\
w^1_{\phi} &= \text{diag}\left(\begin{bmatrix} \frac{I_{y_1} - I_{z_1}}{I_{x_1}} & \cdots & \frac{I_{y_n} - I_{z_n}}{I_{x_n}} \end{bmatrix}\right) \in \mathbb{R}^{n\times n} \\
w^1_{\theta} &= \text{diag}\left(\begin{bmatrix} \frac{I_{z_1} - I_{x_1}}{I_{y_1}} & \cdots & \frac{I_{z_n} - I_{x_n}}{I_{y_n}} \end{bmatrix}\right) \in \mathbb{R}^{n\times n} \\
w^1_{\psi} &= \text{diag}\left(\begin{bmatrix} \frac{I_{x_1} - I_{y_1}}{I_{z_1}} & \cdots & \frac{I_{x_n} - I_{y_n}}{I_{z_n}} \end{bmatrix}\right) \in \mathbb{R}^{n\times n} \\
w^2_{\phi} &= \text{diag}\left(\begin{bmatrix} \frac{1}{I_{x_1}} & \cdots & \frac{1}{I_{x_n}} \end{bmatrix}\right) \in \mathbb{R}^{n\times n} \\
w^2_{\theta} &= \text{diag}\left(\begin{bmatrix} \frac{1}{I_{y_1}} & \cdots & \frac{1}{I_{y_n}} \end{bmatrix}\right) \in \mathbb{R}^{n\times n} \\
w^2_{\psi} &= \text{diag}\left(\begin{bmatrix} \frac{1}{I_{z_1}} & \cdots & \frac{1}{I_{z_n}} \end{bmatrix}\right) \in \mathbb{R}^{n\times n} \\
f_{\phi} &= \begin{bmatrix} \dot{\theta}_1 \dot{\psi}_1 & \cdots & \dot{\theta}_n \dot{\psi}_n \end{bmatrix}^\intercal \in \mathbb{R}^n \\
f_{\theta} &= \begin{bmatrix} \dot{\phi}_1 \dot{\psi}_1 & \cdots & \dot{\phi}_n \dot{\psi}_n \end{bmatrix}^\intercal \in \mathbb{R}^n \\
f_{\psi} &= \begin{bmatrix} \dot{\phi}_1 \dot{\theta}_1 & \cdots & \dot{\phi}_n \dot{\theta}_n \end{bmatrix}^\intercal \in \mathbb{R}^n \\
\tau_{\phi} &= \begin{bmatrix} \tau_{\phi_1} & \cdots & \tau_{\phi_n} \end{bmatrix}^\intercal \in \mathbb{R}^n \\
\tau_{\theta} &= \begin{bmatrix} \tau_{\theta_1} & \cdots & \tau_{\theta_n} \end{bmatrix}^\intercal \in \mathbb{R}^n \\
\tau_{\psi} &= \begin{bmatrix} \tau_{\psi_1} & \cdots & \tau_{\psi_n} \end{bmatrix}^\intercal \in \mathbb{R}^n \\
\delta_{\phi} &= \begin{bmatrix} \delta_{\phi_1} & \cdots & \delta_{\phi_n} \end{bmatrix}^\intercal \in \mathbb{R}^n \\
\delta_{\theta} &= \begin{bmatrix} \delta_{\theta_1} & \cdots & \delta_{\theta_n} \end{bmatrix}^\intercal \in \mathbb{R}^n \\
\delta_{\psi} &= \begin{bmatrix} \delta_{\psi_1} & \cdots & \delta_{\psi_n} \end{bmatrix}^\intercal \in \mathbb{R}^n.
\end{aligned}$$

The orientation angles of the virtual leader composed of roll, pitch, and yaw are represented by $\phi_0 \in \mathbb{R}$, $\theta_0 \in \mathbb{R}$, and $\psi_0 \in \mathbb{R}$, respectively. Similar to the translational dynamics, the rotational dynamics of the leader satisfy the following assumption.

Assumption 4: The dynamics of a virtual leader is bounded such that $\|\ddot{\phi}_0\| \leq \phi_m$, $\|\ddot{\theta}_0\| \leq \theta_m$, and $\|\ddot{\psi}_0\| \leq \psi_m$, where ϕ_m, θ_m, and ψ_m are some known constants.

The communication network in this paper is represented by a general directed graph satisfying the following assumptions.

Assumption 5: The network architecture of the followers consists of at least one directed spanning tree and the leader is linked to at least one agent.

The Laplacian matrix L representing the network topology contains at least one eigenvalue equal to zero, while the remaining eigenvalues have positive real parts. The communication between the leader and agent i is represented by a diagonal B matrix. At least one of the elements of B has a positive real part under Assumption 5. Under this situation, L and B are positive semi-definite matrices.

III. PROPOSED CONTROL DESIGN

A. TRANSLATIONAL CONTROL DESIGN

The tracking errors of formation control are defined by

$$\begin{aligned} e_{x_i} = &\sum_{j=1,i\neq j}^{n} a_{ij}(x_j - x_i) + b_i(x_0 - x_i) \\ &- \sum_{j=1,i\neq j}^{n} a_{ij}(\xi_{x_j} - \xi_{x_i}) - b_i\xi_{x_{0i}} \end{aligned} \tag{13}$$

$$\begin{aligned} e_{y_i} = &\sum_{j=1,i\neq j}^{n} a_{ij}(y_j - y_i) + b_i(y_0 - y_i) \\ &- \sum_{j=1,i\neq j}^{n} a_{ij}(\xi_{y_j} - \xi_{y_i}) - b_i\xi_{y_{0i}} \end{aligned} \tag{14}$$

$$\begin{aligned} e_{z_i} = &\sum_{j=1,i\neq j}^{n} a_{ij}(z_j - z_i) + b_i(z_0 - z_i) \\ &- \sum_{j=1,i\neq j}^{n} a_{ij}(\xi_{z_j} - \xi_{z_i}) - b_i\xi_{z_{0i}}, \end{aligned} \tag{15}$$

where ξ_{x_i}, ξ_{y_i}, and ξ_{z_i} are some constants representing the desired distances between agent i and its neighbour. The desired distances between the leader and followers are represented by constants $\xi_{x_{0i}}$, $\xi_{y_{0i}}$, and $\xi_{z_{0i}}$, respectively. These variables are added in the tracking control to represent the formation shape and to avoid collision between each agent. The objectives of formation control are expressed by

$$\lim_{x\to\infty} e_{x_i}(t) = 0 \tag{16}$$

$$\lim_{x\to\infty} e_{y_i}(t) = 0 \tag{17}$$

$$\lim_{x\to\infty} e_{z_i}(t) = 0, \tag{18}$$

The above errors can be written in the following compact forms

$$e_x = -(L+B)(x - \mathbf{1}_n x_0) + L\xi_x - B\xi_{x_0} \tag{19}$$

$$e_y = -(L+B)(y - \mathbf{1}_n y_0) + L\xi_y - B\xi_{y_0} \tag{20}$$

$$e_z = -(L+B)(z - \mathbf{1}_n z_0) + L\xi_z - B\xi_{z_0}, \tag{21}$$

where

$$\mathbf{1}_n = \begin{bmatrix} 1 & \cdots & 1 \end{bmatrix}^\intercal \in \mathbb{R}^n$$

$$\begin{aligned} e_x &= \begin{bmatrix} e_{x_1} & \cdots & e_{x_n} \end{bmatrix}^\intercal \in \mathbb{R}^n \\ e_y &= \begin{bmatrix} e_{y_1} & \cdots & e_{y_n} \end{bmatrix}^\intercal \in \mathbb{R}^n \\ e_z &= \begin{bmatrix} e_{z_1} & \cdots & e_{z_n} \end{bmatrix}^\intercal \in \mathbb{R}^n \\ \xi_x &= \begin{bmatrix} \xi_{x_1} & \cdots & \xi_{x_n} \end{bmatrix}^\intercal \in \mathbb{R}^n \\ \xi_y &= \begin{bmatrix} \xi_{y_1} & \cdots & \xi_{y_n} \end{bmatrix}^\intercal \in \mathbb{R}^n \\ \xi_z &= \begin{bmatrix} \xi_{z_1} & \cdots & \xi_{z_n} \end{bmatrix}^\intercal \in \mathbb{R}^n \\ \xi_{x_0} &= \begin{bmatrix} \xi_{x_{x_{0_1}}} & \cdots & \xi_{x_{x_{0_n}}} \end{bmatrix}^\intercal \in \mathbb{R}^n \\ \xi_{y_0} &= \begin{bmatrix} \xi_{y_{y_{0_1}}} & \cdots & \xi_{y_{y_{0_n}}} \end{bmatrix}^\intercal \in \mathbb{R}^n \\ \xi_{z_0} &= \begin{bmatrix} \xi_{z_{z_{0_1}}} & \cdots & \xi_{z_{z_{0_n}}} \end{bmatrix}^\intercal \in \mathbb{R}^n. \end{aligned}$$

The formation control of second-order translational dynamics under ideal conditions i.e. without uncertainties can be achieved by applying the following controllers The second-order dynamics of (19), (20), and (21) can be written as

$$\ddot{x} = \Gamma_{x_1}\dot{e}_x + \Gamma_{x_2}e_x \tag{22}$$

$$\ddot{y} = \Gamma_{y_1}\dot{e}_y + \Gamma_{y_2}e_y \tag{23}$$

$$\ddot{z} = \Gamma_{z_1}\dot{e}_z + \Gamma_{z_2}e_z, \tag{24}$$

where

$$\begin{aligned} \Gamma_{x_1} &= \mathrm{diag}\left(\begin{bmatrix} \Gamma_{x_{1_1}} & \cdots & \Gamma_{x_{1_n}} \end{bmatrix}\right) \in \mathbb{R}^{n\times n} \\ \Gamma_{x_2} &= \mathrm{diag}\left(\begin{bmatrix} \Gamma_{x_{2_1}} & \cdots & \Gamma_{x_{2_n}} \end{bmatrix}\right) \in \mathbb{R}^{n\times n} \\ \Gamma_{y_1} &= \mathrm{diag}\left(\begin{bmatrix} \Gamma_{y_{1_1}} & \cdots & \Gamma_{y_{1_n}} \end{bmatrix}\right) \in \mathbb{R}^{n\times n} \\ \Gamma_{y_2} &= \mathrm{diag}\left(\begin{bmatrix} \Gamma_{y_{2_1}} & \cdots & \Gamma_{y_{2_n}} \end{bmatrix}\right) \in \mathbb{R}^{n\times n} \\ \Gamma_{z_1} &= \mathrm{diag}\left(\begin{bmatrix} \Gamma_{z_{1_1}} & \cdots & \Gamma_{z_{1_n}} \end{bmatrix}\right) \in \mathbb{R}^{n\times n} \\ \Gamma_{z_2} &= \mathrm{diag}\left(\begin{bmatrix} \Gamma_{z_{2_1}} & \cdots & \Gamma_{z_{2_n}} \end{bmatrix}\right) \in \mathbb{R}^{n\times n}, \end{aligned}$$

where Γ_{x_1}, Γ_{x_2}, Γ_{y_1}, Γ_{y_2}, Γ_{z_1}, and Γ_{z_2} to be diagonal positive-definite matrices.

The dynamics (22), (23), and (24) can be rewritten in the distributed form as follows

$$\ddot{x}_i = \Gamma_{x_{1_i}}\dot{e}_{x_i} + \Gamma_{x_{2_i}}e_{x_i} \tag{25}$$

$$\ddot{y}_i = \Gamma_{y_{1_i}}\dot{e}_{y_i} + \Gamma_{y_{2_i}}e_{y_i} \tag{26}$$

$$\ddot{z}_i = \Gamma_{z_{1_i}}\dot{e}_{z_i} + \Gamma_{z_{2_i}}e_{z_i}. \tag{27}$$

Let $\mu_i = \begin{bmatrix} \mu_{1_i} & \mu_{2_i} & \mu_{3_i} \end{bmatrix}^\intercal = \begin{bmatrix} \ddot{x}_i & \ddot{y}_i & \ddot{z}_i \end{bmatrix}^\intercal$ is defined to be a virtual control input for agent i. Substituting it to (1), hence

$$z_e\frac{u_{t_i}}{m_i} = J_{t_i}^{-1}\left(\mu_i + (g - \delta_{z_i})z_e\right). \tag{28}$$

By expanding (28), the following set of equations can be generated

$$\begin{aligned} &\mu_{1_i}\cos\theta_i\cos\psi_i + \mu_{2_i}\cos\theta_i\sin\psi_i \\ &\quad -(\mu_{3_i} + g - \delta_{z_i})\sin\theta_i = 0, \end{aligned} \tag{29}$$

$$\begin{aligned} &\mu_{1_i}(\sin\phi_i\sin\theta_i\cos\psi_i - \cos\phi_i\sin\psi_i) \\ &+\mu_{2_i}(\sin\phi_i\sin\theta_i\sin\psi_i + \cos\phi_i\cos\psi_i) \\ &\quad +(\mu_{3_i} + g - \delta_{z_i})\sin\phi_i\cos\theta_i = 0, \end{aligned} \tag{30}$$

$$\mu_{1_i}(\cos\phi_i \sin\theta_i \cos\psi_i + \sin\phi_i \sin\psi_i) + \mu_{2_i}(\cos\phi_i \sin\theta \sin\psi_i - \sin\phi_i \cos\psi_i) + (\mu_{3_i} + g - \delta_{z_i})\cos\phi_i \cos\theta_i = \frac{u_{t_i}}{m_i}. \quad (31)$$

From (29), θ_i can be computed by

$$\theta_i = \arctan\left(\frac{\mu_{1_i}\cos\psi_i + \mu_{2_i}\sin\psi_i}{\mu_{3_i} + g - \delta_{z_i}}\right), \quad (32)$$

for any $\mu_{3_i} + g - \delta_{z_i} \neq 0$. In case $\mu_{3_i} + g - \delta_{z_i} = 0$, it can be obtained from (4) that $w_{z_i}\frac{u_{t_i}}{m_i} = 0$. Note that $w_{z_i} \neq 0$ due to the the value of ϕ_i and θ_i in between $-\frac{\pi}{2}$ to $\frac{\pi}{2}$. It means that $w_{z_i}\frac{u_{t_i}}{m_i} = 0$ only if $u_{t_i} = 0$. In other words, there is no control input in the translational dynamics under this situation. Additionally, it can be generated from (29)

$$\frac{\cos\theta_i}{\sin\theta_i} = \frac{\mu_{3_i} + g - \delta_{z_i}}{\mu_{1_i}\cos\psi_i + \mu_{2_i}\sin\psi_i}. \quad (33)$$

It shows that $\cos\theta_i = 0, \forall\, \mu_{3_i} + g - \delta_{z_i} = 0$. It means that this situation is out of the range of θ_i as stated in Subsection II-A, i.e. $-\frac{\pi}{2} < \theta_i < \frac{\pi}{2}$.

The following is obtained by squaring both sides of (28)

$$\begin{aligned}(\frac{u_{t_i}}{m_i}z_e)^\intercal(\frac{u_{t_i}}{m_i}z_e) &= \left(J_{t_i}^{-1}(\mu_i + (g - \delta_{z_i})z_e)\right)^\intercal \left(J_{t_i}^{-1}(\mu_i + (g - \delta_{z_i})z_e)\right) \\ &= \left(\mu_i + (g - \delta_{z_i})z_e\right)^\intercal \left(\mu_i + (g - \delta_{z_i})z_e\right) \end{aligned} \quad (34)$$

As a result

$$\frac{u_{t_i}}{m_i} = \sqrt{\mu_{1_i}^2 + \mu_{2_i}^2 + (\mu_{1_i} + g - \delta_{z_i})^2} \quad (35)$$

From (30) and (31), the following can be derived

$$\frac{u_{t_i}}{m_i}\sin\phi_i = \mu_{1_i}\sin\psi_i - \mu_{2_i}\cos\psi_i. \quad (36)$$

Substituting (35) to (36), then ϕ_i can be generated by

$$\phi_i = \arcsin\left(\frac{\mu_{1_i}\sin\psi_i - \mu_{2_i}\cos\psi_i}{\sqrt{\mu_{1_i}^2 + \mu_{2_i}^2 + (\mu_{3_i} + g - \delta_{z_i})^2}}\right). \quad (37)$$

Let ϕ_{d_i}, θ_{d_i}, and ψ_{d_i} are the desired ϕ_i, θ_i, and ψ_i, respectively. By following similar steps, both ϕ_{d_i} and θ_{d_i} can be computed under ideal conditions or without the presence of disturbance using

$$\phi_{d_i} = \arcsin\left(\frac{\mu_{1_i}\sin\psi_{d_i} - \mu_{2_i}\cos\psi_{d_i}}{\sqrt{\mu_{1_i}^2 + \mu_{2_i}^2 + (\mu_{3_i} + g)^2}}\right) \quad (38)$$

and

$$\theta_{d_i} = \arctan\left(\frac{\mu_{1_i}\cos\psi_{d_i} + \mu_{2_i}\sin\psi_{d_i}}{\mu_{3_i} + g}\right), \quad (39)$$

for any $\mu_{3_i} + g \neq 0$. Similar to the situation in (33) without disturbance, $\mu_{3_i} + g = 0$ only if $u_{t_i} = 0$.

Both (38) and (39) can be written in a compact form as follows

$$\phi_d = \arcsin\Big(\Big(\text{diag}(\mu_1^2 + \mu_2^2 + (\mu_3 + \mathbf{1}g)^2)\Big)^{-0.5} \Big(\text{diag}(\mu_1)\sin\psi_d - \text{diag}(\mu_2)\cos\psi_d\Big)\Big) \quad (40)$$

and

$$\theta_d = \arctan\Big(\Big(\text{diag}(\mu_3 + \mathbf{1}g)\Big)^{-1}\Big(\text{diag}(\mu_1)\cos\psi_d + \text{diag}(\mu_2)\sin\psi_d\Big)\Big), \quad (41)$$

for any non singular matrix $\text{diag}(\mu_3 + \mathbf{1}g)$, where

$$\begin{aligned}\phi_d &= \begin{bmatrix}\phi_{d_1} & \cdots & \phi_{d_n}\end{bmatrix}^\intercal \in \mathbb{R}^n \\ \theta_d &= \begin{bmatrix}\theta_{d_1} & \cdots & \theta_{d_n}\end{bmatrix}^\intercal \in \mathbb{R}^n \\ \psi_d &= \begin{bmatrix}\psi_{d_1} & \cdots & \psi_{d_n}\end{bmatrix}^\intercal \in \mathbb{R}^n.\end{aligned}$$

The sliding surface of z_i is defined to be

$$s_{z_i} = \lambda_{z_i} e_{z_i} + \dot{e}_{z_i}, \quad (42)$$

where λ_{z_i} is selected to be a positive constant.

The sliding surface (42) can be written in a compact form as follows

$$s_z = \lambda_z e_z + \dot{e}_z, \quad (43)$$

where

$$\begin{aligned}s_z &= \begin{bmatrix}s_{z_1} & \cdots & s_{z_n}\end{bmatrix}^\intercal \in \mathbb{R}^n \\ \lambda_z &= \text{diag}\left(\begin{bmatrix}\lambda_{z_1} & \cdots & \lambda_{z_n}\end{bmatrix}\right) \in \mathbb{R}^{n\times n}.\end{aligned} \quad (44)$$

The dynamics model of (43) can be written as

$$\begin{aligned}\dot{s}_z &= \lambda_z \dot{e}_z + \ddot{e}_z \\ &= \lambda_z \dot{e}_z - (L + B)(\ddot{z} - \mathbf{1}_n \ddot{z}_0).\end{aligned} \quad (45)$$

Substituting (7) to (45), thus

$$\begin{aligned}\dot{s}_z &= \lambda_z \dot{e}_z + \ddot{e}_z \\ &= \lambda_z \dot{e}_z - (L + B)(-g + \delta_z + w_z m^{-1} u_t) \\ &\quad + (L + B)\mathbf{1}_n \ddot{z}_0.\end{aligned} \quad (46)$$

Under Assumption 5, all eigenvalues of $L + B$ have positive real parts. As a result

$$Q_z = P_z(L + B) + (L + B)^\intercal P_z > 0, \quad (47)$$

where $P_z = P_z^\intercal > 0$ is a unique solution of the Lyapunov equation. Before presenting the translational control design, the following notations are defined

$$\begin{aligned}h_{z_1} &= \frac{1}{2}\underline{\sigma}(\gamma_{z_1})\underline{\sigma}(Q_z) - \frac{\bar{\sigma}(\lambda_z)\bar{\sigma}(P_z)\bar{\sigma}(\mathcal{A})}{\underline{\sigma}(D + B)} \\ &\quad - \frac{1}{\alpha_z}\left(1 - \frac{\underline{\sigma}(\lambda_z^2)\underline{\sigma}(P_z)\underline{\sigma}(\mathcal{A})}{\bar{\sigma}(D + B)}\right)^2 \\ h_{z_2} &= \underline{\sigma}(\lambda_z) - \frac{\alpha_z}{2},\ r_z = \begin{bmatrix}\|s_z\| & \|e_z\|\end{bmatrix}^\intercal \\ h_z &= \begin{bmatrix}0 & z_m\bar{\sigma}(P_z)\bar{\sigma}(L + B)\end{bmatrix}^\intercal\end{aligned}$$

$$H_z = \begin{bmatrix} h_{z_1} & 0 \\ 0 & h_{z_2} \end{bmatrix},\ S_z = \begin{bmatrix} P_z & -I_n \\ P_z & \frac{1}{2}I_n \end{bmatrix},$$

where $\underline{\sigma}(.)$ and $\bar{\sigma}(.)$ are the minimum and maximum eigenvalues of $(.)$, respectively. Variable α_z is a positive constant and $I_n \in \mathbb{R}^{n\times n}$ is an identity matrix. The main result of translational control design is briefly outlined in Theorem 3.1.

Theorem 3.1: Consider the dynamical model (4) under Assumptions 1, 2, and 5. The objective of formation control (18) is achieved by selecting

$$u_{t_i} = -\frac{m_i}{w_{z_i}}\Big(\gamma_{z_{1_i}} s_{z_i} + \frac{\lambda_{z_i}}{d_i + b_i}\dot{e}_{z_i} + \gamma_{z_{2_i}} \tanh s_{z_i} - g\Big), \tag{48}$$

where the control gains are chosen to be

$$\begin{aligned} \underline{\sigma}(\gamma_{z_1}) &\geq \frac{2}{\underline{\sigma}(Q_z)}\left(\frac{\bar{\sigma}(\lambda_z)\bar{\sigma}(P_z)\bar{\sigma}(\mathcal{A})}{\underline{\sigma}(D+B)} + \frac{1}{\alpha_z}\left(1 - \frac{\underline{\sigma}(\lambda_z^2)\underline{\sigma}(P_z)\underline{\sigma}(\mathcal{A})}{\bar{\sigma}(D+B)}\right)^2\right) \\ \gamma_{z_{2_i}} &\geq d_z,\ \alpha_z > 0 \\ r_z^\intercal S_z r_z &> \frac{\bar{\sigma}(S_z)\|h_z\|^2}{\underline{\sigma}^2(H_z)}. \end{aligned} \tag{49}$$

Proof: First, u_{t_i} is designed utilizing a conventional SMC as described by

$$u_{t_i} = -\frac{m_i}{w_{z_i}}\Big(\gamma_{z_{1_i}} s_{z_i} + \frac{\lambda_{z_i}}{d_i + b_i}\dot{e}_{z_i} + \gamma_{z_{2_i}} \mathrm{sgn}(s_{z_i}) - g\Big). \tag{50}$$

It can be written in a compact form as

$$u_t = -\frac{m}{w_z}\Big(\gamma_{z_1} s_z + (D+B)^{-1}\lambda_z \dot{e}_z + \gamma_{z_2}\mathrm{sgn}(s_z) - \mathbf{1}_n g\Big). \tag{51}$$

Substituting (51) to (46), thus

$$\begin{aligned} \dot{s}_z = \lambda_z \dot{e}_z + (L+B)\mathbf{1}_n \ddot{z}_0 - (L+B)(\gamma_{z_1} s_z \\ + (D+B)^{-1}\lambda_z \dot{e}_z + \gamma_{z_2}\mathrm{sgn}(s_z) + \delta_z). \end{aligned} \tag{52}$$

Consider now the following Lyapunov function candidate

$$V_z = \frac{1}{2}s_z^\intercal P_z s_z + \frac{1}{2}e_z^\intercal e_z. \tag{53}$$

The time-derivative of (53) is

$$\begin{aligned} \dot{V}_z &= s_z^\intercal P_z \dot{s}_z + e_z^\intercal \dot{e}_z \\ &= -s_z^\intercal P_z (L+B)\big(\gamma_{z_1} s_z + (D+B)^{-1}\lambda_z \dot{e}_z \\ &\quad + \gamma_{z_2}\mathrm{sgn}(s_z) + \delta_z\big) + s_z^\intercal P_z (L+B)\mathbf{1}_n \ddot{z}_0 \\ &\quad + s_z^\intercal P_z \lambda_z \dot{e}_z + e_z^\intercal \dot{e}_z \\ &\leq -\frac{1}{2}s_z^\intercal \gamma_{z_1} Q_z s_z - s_z^\intercal P_z (D - \mathcal{A} + B) \\ &\quad (D+B)^{-1}\lambda_z \dot{e}_z + s_z^\intercal P_z (L+B)\mathbf{1}_n \ddot{z}_0 \\ &\quad + s_z^\intercal P_z \lambda_z \dot{e}_z + e_z^\intercal (s_z - \lambda_z e_z) \\ &\leq -\frac{1}{2}s_z^\intercal \gamma_{z_1} Q_z s_z - e_z^\intercal \lambda_z e_z + s_z^\intercal P_z \mathcal{A}(D+B)^{-1} \\ &\quad \lambda_z (s_z - \lambda_z e_z) + s_z^\intercal P_z (L+B)\mathbf{1}_n \ddot{z}_0 + e_z^\intercal s_z \\ &\leq -\frac{1}{2}s_z^\intercal \gamma_{z_1} Q_z s_z - e_z^\intercal \lambda_z e_z + s_z^\intercal P_z \mathcal{A}(D+B)^{-1} \\ &\quad \lambda_z (s_z - \lambda_z e_z) + s_z^\intercal P_z (L+B)\mathbf{1}_n \ddot{z}_0 + s_z^\intercal e_z \\ &\leq -\frac{1}{2}s_z^\intercal \gamma_{z_1} Q_z s_z - e_z^\intercal \lambda_z e_z + s_z^\intercal P_z (L+B)\mathbf{1}_n \ddot{z}_0 \\ &\quad + s_z^\intercal \lambda_z P_z \mathcal{A}(D+B)^{-1} s_z + s_z^\intercal \left(I - \frac{\lambda_z^2 P_z \mathcal{A}}{D+B}\right) e_z \\ &\leq -\frac{1}{2}\underline{\sigma}(\gamma_{z_1})\underline{\sigma}(Q_z)\|s_z\|^2 - \underline{\sigma}(\lambda_z)\|e_z\|^2 + z_m \bar{\sigma}(P_z) \\ &\quad \bar{\sigma}(L+B)\|s_z\| + \frac{\bar{\sigma}(\lambda_z)\bar{\sigma}(P_z)\bar{\sigma}(\mathcal{A})}{\underline{\sigma}(D+B)}\|s_z\|^2 \\ &\quad + \left(1 - \frac{\underline{\sigma}(\lambda_z^2)\underline{\sigma}(P_z)\underline{\sigma}(\mathcal{A})}{\bar{\sigma}(D+B)}\right)^2 \frac{\|s_z\|^2}{\alpha_z} + \frac{\alpha_z \|e_z\|^2}{2} \\ &\leq -h_{z_1}\|s_z\|^2 - h_{z_2}\|e_z\|^2 + z_m \bar{\sigma}(P_z)\bar{\sigma}(L+B)\|s_z\| \\ &\leq -\underline{\sigma}(H_z)\|r_z\|^2 + h_z\|r_z\|. \end{aligned} \tag{54}$$

It is obvious to see that $\dot{V}_z \leq 0$ if and only if by selecting $\underline{\sigma}(\gamma_{z_1})$ and $\underline{\sigma}(\lambda_z)$ to be some positive constants such that $H_z \geq 0$ and

$$\|r_z\| > \frac{h_z}{\underline{\sigma}(H_z)}. \tag{55}$$

From (53), it can be seen that $\dot{V}_z \leq 0$ with sufficient large V_z such that (55) holds. The Lyapunov function (53) can be rewritten as

$$V_z = \frac{1}{2}r_z^\intercal S_z r_z. \tag{56}$$

The lower and upper bound of (56) are expressed by

$$\frac{1}{2}\underline{\sigma}(S_z)\|r_z\|^2 \leq V_z \leq \frac{1}{2}\bar{\sigma}(S_z)\|r_z\|^2. \tag{57}$$

Hence

$$V_z > \frac{\bar{\sigma}(S_z)\|h_z\|^2}{2\underline{\sigma}^2(H_z)} \tag{58}$$

implies (55).

The chattering issue in conventional SMC is attenuated by employing an approximation of the $\mathrm{sgn}(s_{z_i})$ value through the utilization of a hyperbolic tangent function, denoted as $\tanh(s_{z_i})$. Therefore, the original sign function in (50) is substituted with $\tanh(s_{z_i})$ as indicated in (48). The hyperbolic tangent function is characterized by its smooth nature, expressed mathematically as

$$\tanh(S_{z_i}(k)) = \frac{e^{S_{z_i}(k)} - e^{-S_{z_i}(k)}}{e^{S_{z_i}(k)} + e^{-S_{z_i}(k)}}, \tag{59}$$

and has the following properties as outlined by

$$\tanh(S_{z_i}(k)) = \begin{cases} -1, \text{ for negative big } S_{z_i}(k) \\ 0, \text{ for } S_{z_i}(k) = 0 \\ 1, \text{ for positive big } S_{z_i}(k) \end{cases}. \tag{60}$$

More details of this approximating method can be found in [13], [14]. The proof is thus completed. ■

B. ROTATIONAL CONTROL DESIGN

The error of dynamics (8), (9), and(10) in the networked environment can be written as follows

$$e_{\phi_i} = \phi_i - \phi_{d_i} \tag{61}$$
$$e_{\theta_i} = \theta_i - \theta_{d_i} \tag{62}$$
$$e_{\psi_i} = \psi_i - \psi_{d_i} \tag{63}$$

The main objective of the agent i is to synchronize its angles with the leader and connected neighbor as represented by

$$\lim_{t\to\infty} \begin{bmatrix} e_{\phi_i} & e_{\theta_i} & e_{\psi_i} \end{bmatrix}^\intercal = \mathbf{0}_3, \tag{64}$$

where $\mathbf{0}_3 \in \mathbb{R}^n$ is a zero vector. The global neighborhood synchronization error can be written in compact forms as

$$e_\phi = \phi - \phi_d \tag{65}$$
$$e_\theta = \theta - \theta_d \tag{66}$$
$$e_\psi = \psi - \psi_d. \tag{67}$$

The sliding surfaces of rotational dynamics of agent i are expressed by the following equations

$$s_{\phi_i} = \lambda_{\phi_i} e_{\phi_i} + \dot{e}_{\phi_i} \tag{68}$$
$$s_{\theta_i} = \lambda_{\theta_i} e_{\theta_i} + \dot{e}_{\theta_i} \tag{69}$$
$$s_{\psi_i} = \lambda_{\psi_i} e_{\psi_i} + \dot{e}_{\psi_i} \tag{70}$$

Similar to the sliding surface of z_i. It is obvious to see that

$$\dot{e}_{\phi_i} = -\lambda_{\phi_i} e_{\phi_i}$$
$$\dot{e}_{\theta_i} = -\lambda_{\theta_i} e_{\theta_i}$$
$$\dot{e}_{\psi_i} = -\lambda_{\psi_i} e_{\psi_i}$$

are stable if s_{ϕ_i}, s_{θ_i}, and s_{ψ_i} are zero for any positive constants λ_{ϕ_i}, λ_{θ_i}, and λ_{ψ_i}. In this situation, $\dot{e}_{\phi_i} = -\lambda_{\phi_i} e_{\phi_i}$, $\dot{e}_{\theta_i} = -\lambda_{\theta_i} e_{\theta_i}$, and $\dot{e}_{\psi_i} = -\lambda_{\psi_i} e_{\psi_i}$. It means that the error dynamics (61), (62), and (63) are achieved by converging s_{ϕ_i}, s_{θ_i}, and s_{ψ_i} to zero.

The sliding surface (68), (69), and (70) can be written in a compact form as

$$s_\phi = \lambda_\phi e_\phi + \dot{e}_\phi \tag{71}$$
$$s_\theta = \lambda_\theta e_\theta + \dot{e}_\theta \tag{72}$$
$$s_\psi = \lambda_\psi e_\psi + \dot{e}_\psi, \tag{73}$$

where

$$s_\phi = \begin{bmatrix} s_{\phi_1} & \cdots & s_{\phi_n} \end{bmatrix}^\intercal \in \mathbb{R}^n$$
$$s_\theta = \begin{bmatrix} s_{\theta_1} & \cdots & s_{\theta_n} \end{bmatrix}^\intercal \in \mathbb{R}^n$$
$$s_\psi = \begin{bmatrix} s_{\psi_1} & \cdots & s_{\psi_n} \end{bmatrix}^\intercal \in \mathbb{R}^n$$
$$\lambda_\phi = \text{diag}\left(\begin{bmatrix} \lambda_{\phi_1} & \cdots & \lambda_{\phi_n} \end{bmatrix}\right) \in \mathbb{R}^{n\times n}$$
$$\lambda_\theta = \text{diag}\left(\begin{bmatrix} \lambda_{\theta_1} & \cdots & \lambda_{\theta_n} \end{bmatrix}\right) \in \mathbb{R}^{n\times n}$$
$$\lambda_\psi = \text{diag}\left(\begin{bmatrix} \lambda_{\psi_1} & \cdots & \lambda_{\psi_n} \end{bmatrix}\right) \in \mathbb{R}^{n\times n}.$$

The dynamics model of (71), (72), and (73) can be written as

$$\dot{s}_\phi = \lambda_\phi \dot{e}_\phi + \ddot{e}_\phi$$
$$= \lambda_\phi \dot{e}_\phi + \ddot{\phi} - \ddot{\phi}_d \tag{74}$$
$$\dot{s}_\theta = \lambda_\theta \dot{e}_\theta + \ddot{e}_\theta$$
$$= \lambda_\theta \dot{e}_\theta + \ddot{\theta} - \ddot{\theta}_d \tag{75}$$
$$\dot{s}_\psi = \lambda_\psi \dot{e}_\psi + \ddot{e}_\psi$$
$$= \lambda_\psi \dot{e}_\psi + \ddot{\psi} - \ddot{\psi}_d \tag{76}$$

The main result of the rotational control design is summarized in the following theorem.

Theorem 3.2: Consider the dynamical model (8), (9), and (10) under Assumptions 3, 4, and 5. The objective of synchronization control (64) is achieved by selecting

$$\tau_{\phi_i} = -{w^2_{\phi_i}}^{-1}\Big(w^1_{\phi_i} f_{\phi_i} + \gamma_{\phi_{1_i}} s_{\phi_i} + \gamma_{\phi_{2_i}} \tanh s_{\phi_i} + \ddot{\phi}_{d_i}\Big) \tag{77}$$
$$\tau_{\theta_i} = -{w^2_{\theta_i}}^{-1}\Big(w^1_{\theta_i} f_{\theta_i} + \gamma_{\theta_{1_i}} s_{\theta_i} + \gamma_{\theta_{2_i}} \tanh s_{\theta_i} + \ddot{\theta}_{d_i}\Big) \tag{78}$$
$$\tau_{\psi_i} = -{w^2_{\psi_i}}^{-1}\Big(w^1_{\psi_i} f_{\psi_i} + \gamma_{\psi_{1_i}} s_{\psi_i} + \gamma_{\psi_{2_i}} \tanh s_{\psi_i} + \ddot{\psi}_{d_i}\Big), \tag{79}$$

where

$$\gamma_{\phi_{1_i}} > 0,\ \gamma_{\theta_{1_i}} > 0,\ \gamma_{\psi_{1_i}} > 0$$
$$\gamma_{\phi_{2_i}} \geq d_{\phi_i},\ \gamma_{\theta_{2_i}} \geq d_{\theta_i},\ \gamma_{\psi_{2_i}} \geq d_{\psi_i}$$

Proof: First, τ_{ϕ_i}, τ_{θ_i}, and τ_{ψ_i} are designed using a conventional SMC as expressed by

$$\tau_{\phi_i} = -{w^2_{\phi_i}}^{-1}\Big(w^1_{\phi_i} f_{\phi_i} + \gamma_{\phi_{1_i}} s_{\phi_i} + \gamma_{\phi_{2_i}} \text{sgn}(s_{\phi_i}) + \ddot{\phi}_{d_i}\Big) \tag{80}$$
$$\tau_{\theta_i} = -{w^2_{\theta_i}}^{-1}\Big(w^1_{\theta_i} f_{\theta_i} + \gamma_{\theta_{1_i}} s_{\theta_i} + \gamma_{\theta_{2_i}} \text{sgn}(s_{\theta_i}) + \ddot{\theta}_{d_i}\Big) \tag{81}$$
$$\tau_{\psi_i} = -{w^2_{\psi_i}}^{-1}\Big(w^1_{\psi_i} f_{\psi_i} + \gamma_{\psi_{1_i}} s_{\psi_i} + \gamma_{\psi_{2_i}} \text{sgn}(s_{\psi_i}) + \ddot{\psi}_{d_i}\Big), \tag{82}$$

It can be written in a compact form as

$$\tau_\phi = -w^{2\,-1}_\phi\Big(w^1_\phi f_\phi + \gamma_{\phi_1} s_\phi + \gamma_{\phi_2} \text{sgn}(s_\phi) + \ddot{\phi}_{d_i}\Big) \tag{83}$$
$$\tau_\theta = -w^{2\,-1}_\theta\Big(w^1_\theta f_\theta + \gamma_{\theta_1} s_\theta + \gamma_{\theta_2} \text{sgn}(s_\theta) + \ddot{\theta}_{d_i}\Big) \tag{84}$$
$$\tau_\psi = -w^{2\,-1}_\psi\Big(w^1_\psi f_\psi + \gamma_{\psi_1} s_\psi + \gamma_{\psi_2} \text{sgn}(s_\psi) + \ddot{\psi}_{d_i}\Big), \tag{85}$$

Substituting (83) to (74), (84) to (75), and (85) to (76) thus

$$\dot{s}_\phi = \delta_\phi - \gamma_{\phi_1} s_\phi - \gamma_{\phi_2} \text{sgn}(s_\phi) \tag{86}$$
$$\dot{s}_\theta = \delta_\theta - \gamma_{\theta_1} s_\theta - \gamma_{\theta_2} \text{sgn}(s_\theta) \tag{87}$$
$$\dot{s}_\psi = \delta_\psi - \gamma_{\psi_1} s_\psi - \gamma_{\psi_2} \text{sgn}(s_\psi). \tag{88}$$

Consider now the following Lyapunov function candidates

$$V_\phi = \frac{1}{2} s^\intercal_\phi P_\phi s_\phi \tag{89}$$

$$V_\theta = \frac{1}{2} s_\theta^\intercal P_\theta s_\theta \tag{90}$$

$$V_\psi = \frac{1}{2} s_\psi^\intercal P_\psi s_\psi. \tag{91}$$

The time-derivative of (89) is

$$\begin{aligned}\dot{V}_\phi &= s_\phi^\intercal P_\phi \dot{s}_\phi \\ &= s_\phi^\intercal P_\phi (\delta_\phi - \gamma_{\phi_1} s_\phi - \gamma_{\phi_2} \text{sgn}(s_\phi)) \\ &\leq -s_\phi^\intercal P_\phi \gamma_{\phi_1} s_\phi + s_\phi^\intercal P_\phi (d_\phi - \gamma_{\phi_2} \text{sgn}(s_\phi)) \\ &\leq -s_\phi^\intercal P_\phi \gamma_{\phi_1} s_\phi \leq 0. \end{aligned} \tag{92}$$

By following a similar way, the time-derivative of (90) and (91) can be obtained as follows

$$\dot{V}_\theta \leq -s_\theta^\intercal P_\theta \gamma_{\theta_1} s_\theta \leq 0 \tag{93}$$

$$\dot{V}_\psi \leq -s_\psi^\intercal P_\psi \gamma_{\psi_1} s_\psi \leq 0. \tag{94}$$

By following a similar method in Theorem 3.1, the chattering issue observed in conventional SMC can be attenuated by approximating the values of the $\text{sgn}(s_{\phi_i})$, $\text{sgn}(s_{\theta_i})$, and $\text{sgn}(s_{\psi_i})$ using hyperbolic tangent functions $\tanh(s_{\phi_i})$, $\tanh(s_{\theta_i})$, and $\tanh(s_{\psi_i})$, respectively. Therefore, the sign functions in (80), (81), and (82) are replaced by $\tanh(s_{\phi_i})$ as represented by (77), (78), and (79), respectively. The proof is thus completed. ■

IV. SIMULATION RESULTS

This section assesses the effectiveness of the proposed formation control protocols through numerical evaluations. The simulation involves a configuration with a single active virtual leader and four followers. Heterogeneous UAVs characterized by distinct parameters are utilized in the simulation. The specific parameters of the multi-UAVs employed are outlined in the following table.

TABLE 1: Specifications of Quadrotor UAVs [46], [47]

Parameter Notation	Value (UAVs 1 & 2)	Value (UAVs 3 & 4)
m	1 kg	2.4 kg
I_x	0.0069 kg · m^2	0.16 kg · m^2
I_y	0.0069 kg · m^2	0.16 kg · m^2
I_z	0.0129 kg · m^2	0.32 kg · m^2

Figure 1 depicts the communication process for each agent and leader.

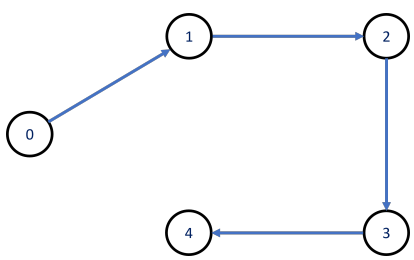

FIGURE 1: The network topology of four agents and one leader

Matrices L and B matrices of the network can be computed from the above topology as expressed by

$$L = \begin{bmatrix} 0 & 0 & 0 & 0 \\ -1 & 1 & 0 & 0 \\ 0 & -1 & 1 & 0 \\ 0 & 0 & -1 & 1 \end{bmatrix}, \; B = \begin{bmatrix} 1 & 0 & 0 & 0 \\ 0 & 0 & 0 & 0 \\ 0 & 0 & 0 & 0 \\ 0 & 0 & 0 & 0 \end{bmatrix}.$$

Different external disturbances are introduced into the closed-loop systems of individual agents as expressed by

$$\begin{aligned} \delta_z &= 0.1 \begin{bmatrix} -1.2\sin(t) & 0.5\cos(t) & -0.3\cos(t) & \sin(t) \end{bmatrix}^\intercal \\ \delta_\phi &= 0.1 \begin{bmatrix} 0.7\sin(t) & 0.4\sin(t) & -\cos(t) & \sin(t) \end{bmatrix}^\intercal \\ \delta_\theta &= 0.1 \begin{bmatrix} -0.2\cos(t) & -\sin(t) & 0.3\cos(t) & 1.2\cos(t) \end{bmatrix}^\intercal \\ \delta_\psi &= 0.1 \begin{bmatrix} 0.2\sin(t) & -\sin(t) & 0.6\cos(t) & 0.6\cos(t) \end{bmatrix}^\intercal. \end{aligned}$$

The specified initial conditions for the leader and followers in this simulation are as follows

$$\begin{aligned} x_0(0) = -0.1, \; y_0(0) = -0.3, \; z_0(0) = 0 \\ x(0) = \begin{bmatrix} -1 & 2 & -4 & 5 \end{bmatrix}^\intercal \\ y(0) = \begin{bmatrix} 2 & -4 & 5 & -1 \end{bmatrix}^\intercal \\ z(0) = \begin{bmatrix} 0 & 0 & 0 & 0 \end{bmatrix}^\intercal. \end{aligned}$$

The desired formation of the connected agents is represented by

$$\begin{aligned} \xi_{x_0} = 2, \; \xi_{y_0} = 3, \; \xi_{z_0} = 0 \\ \xi_x = \begin{bmatrix} 2 & 4 & 6 & 8 \end{bmatrix}^\intercal \\ \xi_y = \begin{bmatrix} 3 & 6 & 9 & 12 \end{bmatrix}^\intercal \\ \xi_z = \begin{bmatrix} 0 & 0 & 0 & 0 \end{bmatrix}^\intercal. \end{aligned}$$

To achieve the desired formation, the control gains are chosen to be

$$\begin{aligned} \Gamma_{x_1} &= 10^3 I_4, \; \Gamma_{x_2} = 10^2 I_4 \\ \Gamma_{y_1} &= 10^3 I_4, \; \Gamma_{y_2} = 10^2 I_4 \\ \Gamma_{z_1} &= 10^3 I_4, \; \Gamma_{z_2} = 10^2 I_4 \\ \gamma_{z_1} &= 10^3 I_4, \; \gamma_{z_2} = 0.15 I_4, \; \lambda_z = I_4 \\ \gamma_{\phi_1} &= 10^3 \text{diag}\left(\begin{bmatrix} 2 & 2 & 1 & 1 \end{bmatrix}\right) \\ \gamma_{\phi_2} &= \text{diag}\left(\begin{bmatrix} 0.14 & 0.14 & 0.14 & 0.28 \end{bmatrix}\right) \\ \lambda_\phi &= 10^2 \text{diag}\left(\begin{bmatrix} 20 & 20 & 1 & 1 \end{bmatrix}\right) \\ \gamma_{\theta_1} &= 10^3 \text{diag}\left(\begin{bmatrix} 2 & 2 & 1 & 1 \end{bmatrix}\right) \\ \gamma_{\theta_2} &= \text{diag}\left(\begin{bmatrix} 0.14 & 0.14 & 0.14 & 0.28 \end{bmatrix}\right) \\ \lambda_\theta &= 10^2 \text{diag}\left(\begin{bmatrix} 20 & 20 & 1 & 1 \end{bmatrix}\right) \\ \gamma_{\psi_1} &= 10^4 \text{diag}\left(\begin{bmatrix} 2 & 2 & 5 & 5 \end{bmatrix}\right) \\ \gamma_{\theta_2} &= \text{diag}\left(\begin{bmatrix} 0.14 & 0.14 & 0.14 & 0.28 \end{bmatrix}\right) \\ \lambda_\psi &= 10^2 \text{diag}\left(\begin{bmatrix} 20 & 20 & 1 & 1 \end{bmatrix}\right) \end{aligned} \tag{95}$$

A visual representation of the successful convergence of tracking errors within the attitude dynamics states such as roll, pitch, and yaw, for the leader and each agent is presented in Figure 2. Initially, during the formation of the leader and agents, fluctuations are observed due to various

initial positions along the x and y axes. After 30s of travel, these fluctuations dissipate, indicating the achievement of the designated x, y, and z positions. This implies that the effectiveness of distributed control inputs (77), (78), and (79) to stabilize the inner loop systems.

Figures 3 and 4 illustrate the formation control of multi-UAVs along the x, y, and z axes. The formation control for every axis can be seen in Figure 3. It shows that agent i and leader move from different initial conditions to the desired formation. In this simulation, the desired distance along the x and y axes are set to be 2m and 3m, respectively. It can be seen that the desired formation is closely approached within 40s, after which it is consistently maintained throughout the formation. This visual narrative demonstrates the precision of the control strategy to maintain multiple heterogeneous UAV movement coordination within the multi-agent systems. For a more convenient presentation, Figure 4 illustrates the multiple UAV movements in 3D space.

The control input profiles are depicted in Figure 6. To characterize the application setting, the absolute value of the torque magnitude for agent i is constrained to be no greater than $18kg \cdot m^2/s^2$. The torques observed during the transient phase of formation control do not exhibit extreme oscillations, as shown in the zoom-in box in Figure 6. Furthermore, they gradually diminish in sync with the reduction of formation error. This behavior is reasonable, considering that agent i starts from diverse initial positions, and only agent 1 is directly linked to the leader.

The above conclusion is also emphasized by the formation errors of agent i along x, y, and z axes presented in Figure 5. It shows a consistent reduction of tracking errors toward zero. In other words, the formation consensus is achieved as concluded in Theorem 3.1. Moreover, both Figures 2 and 3 also show the performance of the proposed control protocols to handle unknown external disturbances affecting the translational and rotational dynamics of every agent.

To assess the performance of the proposed scheme, a series of simulations were conducted, comparing it with conventional SMC. All translational and rotational states are maintained using the same gains using conventional SMC, as illustrated in Figure 7 and 8. However, small chattering is observed in control inputs, as shown in Figure 9. This phenomenon arises due to the small gains in robust terms, such as γ_{z_2}, γ_{ϕ_2}, γ_{θ_2}, and γ_{ψ_2}. The selection of these robust terms is crucial, as they significantly influence the control input profiles. Inappropriate gains may cause chattering issues, rendering the control scheme impractical for real-world applications. To evaluate this aspect, the robust gains are increased by 50 times. Although conventional SMC can still manage all translational and rotational states, achieving the desired formation requires extreme oscillatory control inputs, as depicted in Figures 10-12. Such oscillations are not feasible due to hardware constraints.

In contrast, by increasing the robust term gains by 50 times using the proposed design, the desired formation is still achieved without experiencing extreme chattering in control inputs, as demonstrated in Figures 13-15. These results demonstrate the advantages of the proposed control protocol, as outlined in Theorem 3.1 and 3.2. The proposed approach effectively attenuates chattering issues while maintaining stable and precise formation control, even under uncertainties. This enhanced performance highlights the superiority of the proposed scheme over conventional SMC, particularly in real-world UAV applications where robustness and stability are paramount.

V. CONCLUSIONS

A distributed robust formation control framework for a fleet of heterogeneous UAVs with six degrees of freedom (6-DOF) operating in the presence of uncertain and time-varying disturbances is introduced in this paper. The proposed design is tailored to the underactuated UAVs connected by a directed graph. Each agent's movement is regulated through a feedback controller that relies on relative position and velocity measurements concerning both connected agents and a designated leader. In this scheme, only at least a minimum of one agent is required to establish a connection with the leader for this control scheme to function effectively. This framework has robust terms to handle the impact of uncertain external disturbances that affect both the translational and rotational dynamics of each agent. A rigorous mathematical proof is provided to establish the efficacy of the proposed controller. The numerical examples are presented to demonstrate and validate the performance of the proposed design. It would be exciting to explore other scenarios in future work such as time-varying payloads, cyber-attacks, and fault-tolerance factors. Furthermore, it also would be interesting to extend this research by addressing challenges related to obstacle avoidance and exploring its implementation in real-world applications.

ACKNOWLEDGMENT

The work is supported by the King Fahd University of Petroleum and Minerals (KFUPM).

REFERENCES

[1] Reza Shakeri, Mohammed Ali Al-Garadi, Ahmed Badawy, Amr Mohamed, Tamer Khattab, Abdulla Khalid Al-Ali, Khaled A Harras, and Mohsen Guizani. Design challenges of multi-uav systems in cyber-physical applications: A comprehensive survey and future directions. IEEE Communications Surveys & Tutorials, 21(4):3340–3385, 2019.

[2] Haijun Wang, Haitao Zhao, Jiao Zhang, Dongtang Ma, Jiaxun Li, and Jibo Wei. Survey on unmanned aerial vehicle networks: A cyber physical system perspective. IEEE Communications Surveys & Tutorials, 22(2):1027–1070, 2019.

[3] Allahyar Montazeri, Aydin Can, and Imil Hamda Imran. Unmanned aerial systems: autonomy, cognition, and control. In Unmanned aerial systems, pages 47–80. Elsevier, 2021.

[4] Thomas Burrell, Craig West, Stephens D Monk, Allahyar Montezeri, and C James Taylor. Towards a cooperative robotic system for autonomous pipe cutting in nuclear decommissioning. In 2018 UKACC 12th International Conference on Control (CONTROL), pages 283–288. IEEE, 2018.

[5] Srikanth Goli, Dilek Funda Kurtuluş, Luai M Alhems, Azhar M Memon, and Imil Hamda Imran. Experimental study on efficient propulsion system for multicopter uav design applications. Results in Engineering, 20:101555, 2023.

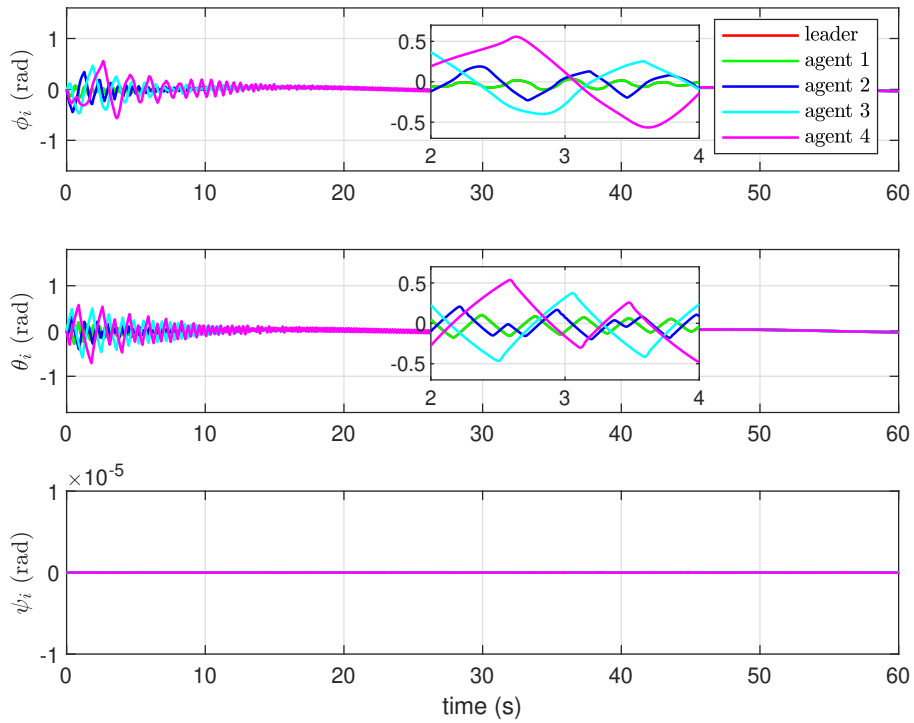

FIGURE 2: The profile of ϕ_i, θ_i and ψ_i

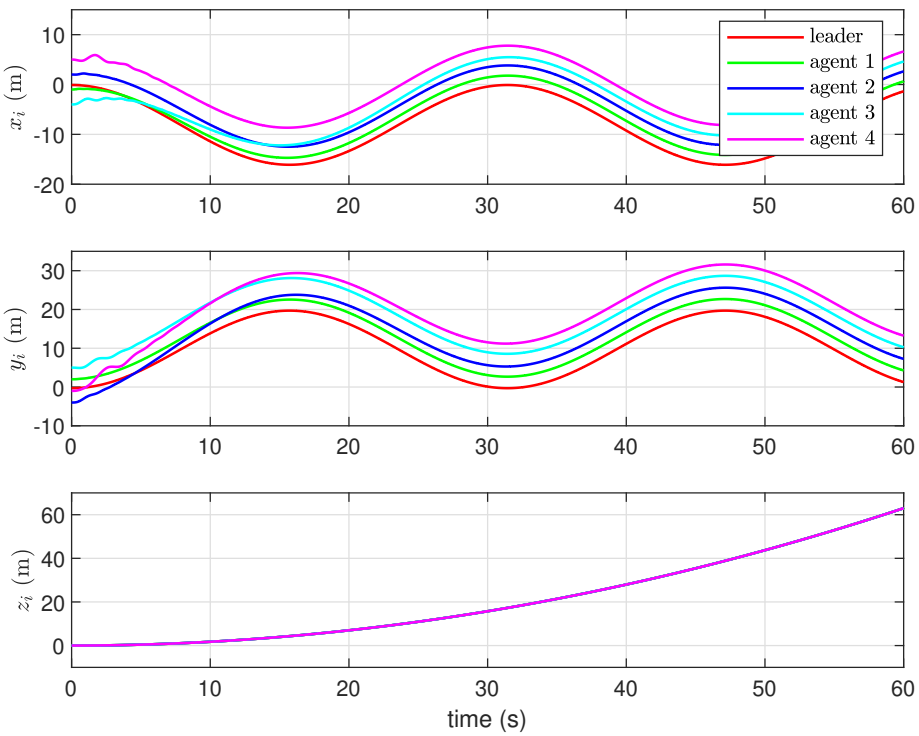

FIGURE 3: The profile of x_i, y_i and z_i

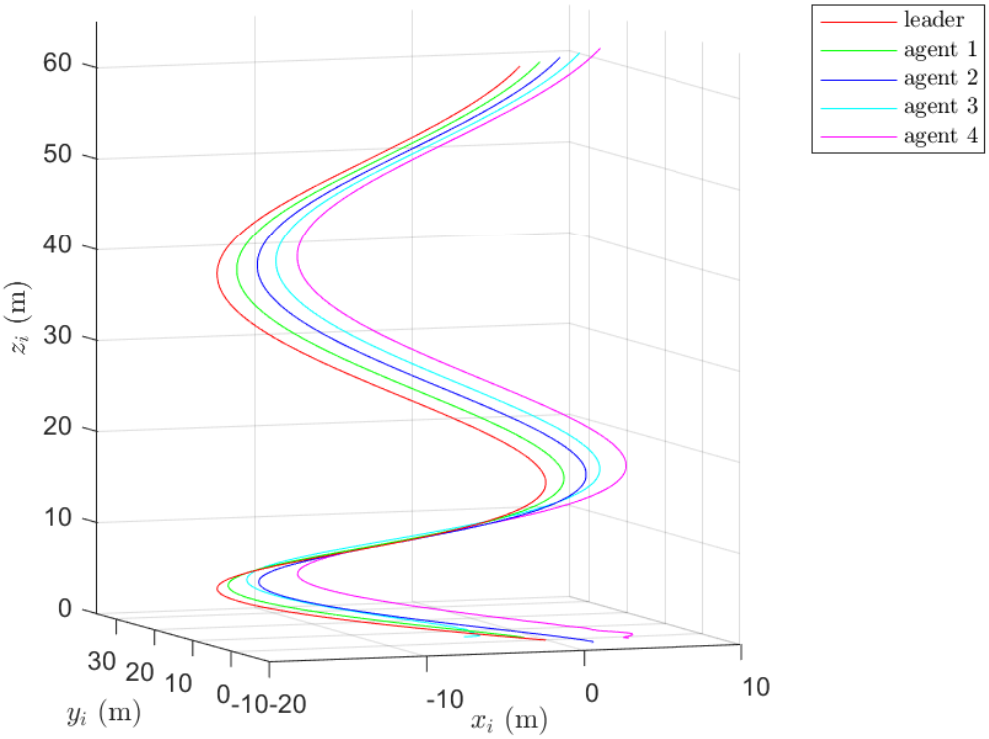

FIGURE 4: The profile of x_i, y_i and z_i in 3D space

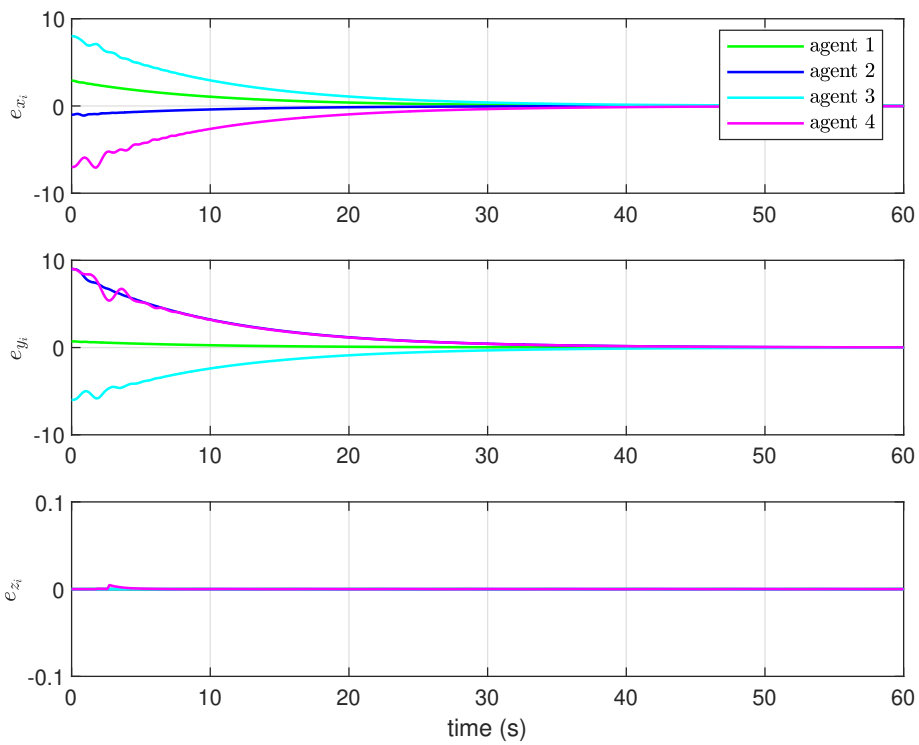

FIGURE 5: The profile of formation error

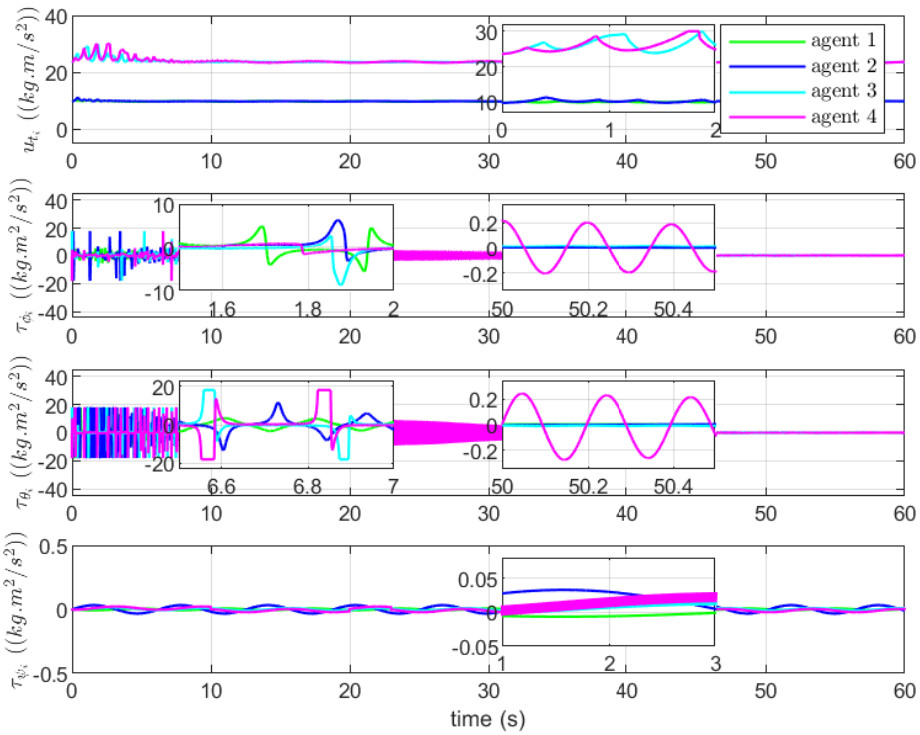

FIGURE 6: The profile of control inputs

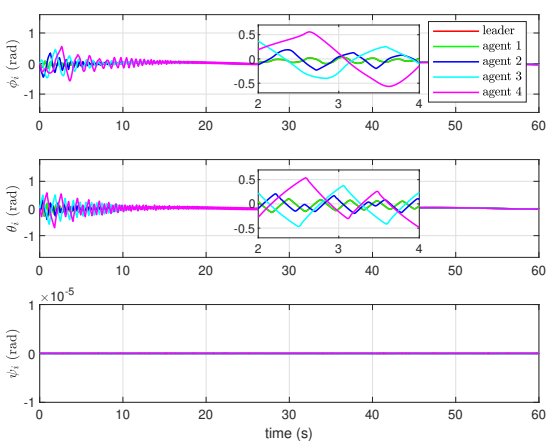

FIGURE 7: The profile of ϕ_i, θ_i and ψ_i using conventional SMC

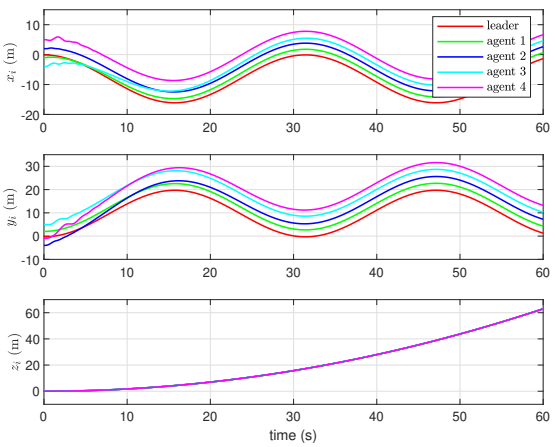

FIGURE 8: The profile of x_i, y_i and z_i using conventional SMC

[6] Zhao Shulong, An Honglei, Zhang Daibing, and Shen Lincheng. A new feedback linearization lqr control for attitude of quadrotor. In 2014 13th International Conference on Control Automation Robotics & Vision (ICARCV), pages 1593–1597. IEEE, 2014.

[7] Shahida Khatoon, Dhiraj Gupta, and LK Das. Pid & lqr control for a quadrotor: Modeling and simulation. In 2014 international conference on advances in computing, communications and informatics (ICACCI), pages 796–802. IEEE, 2014.

[8] Atheer Salih, Mahmoud Moghavvemi, and Haider AF Mohamed. Flight pid controller design for a uav quadrotor. Scientific Research and Essays (SRE), 5(23):3660–3667, 2010.

[9] Axel Reizenstein. Position and trajectory control of a quadcopter using pid and lq controllers. Master's thesis, Linköping University (Sweden), 2017.

[10] Faraz Ahmad, Pushpendra Kumar, Anamika Bhandari, and Pravin P Patil. Simulation of the quadcopter dynamics with lqr based control. Materials Today: Proceedings, 24:326–332, 2020.

[11] Qing-Li Zhou, Youmin Zhang, Camille-Alain Rabbath, and Didier Theilliol. Design of feedback linearization control and reconfigurable control allocation with application to a quadrotor uav. In 2010 Conference on Control and Fault-Tolerant Systems (SysTol), pages 371–376. IEEE, 2010.

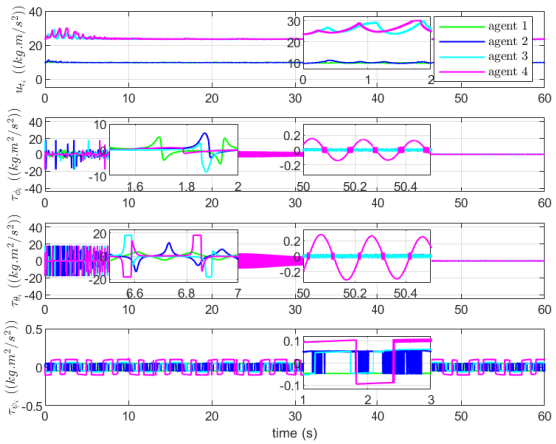

FIGURE 9: The profile of control inputs using conventional SMC

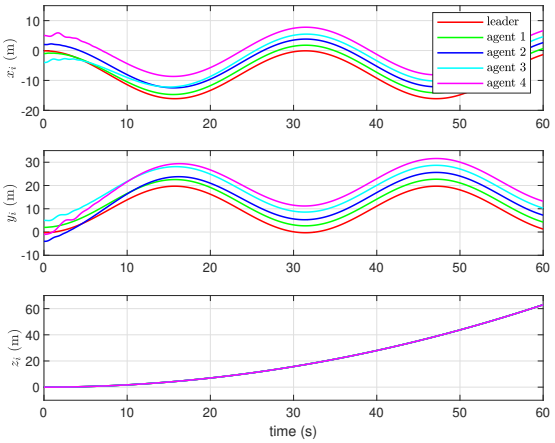

FIGURE 11: The profile of x_i, y_i and z_i using conventional SMC

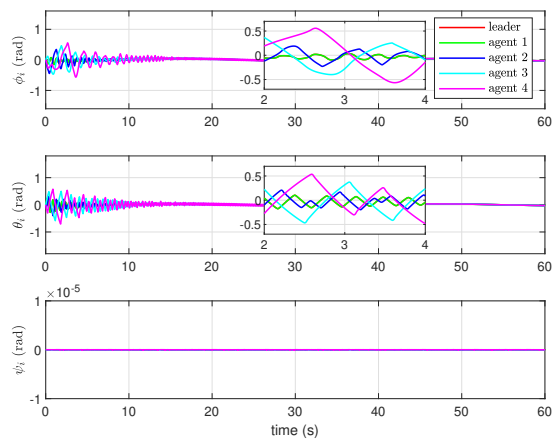

FIGURE 10: The profile of ϕ_i, θ_i and ψ_i using conventional SMC

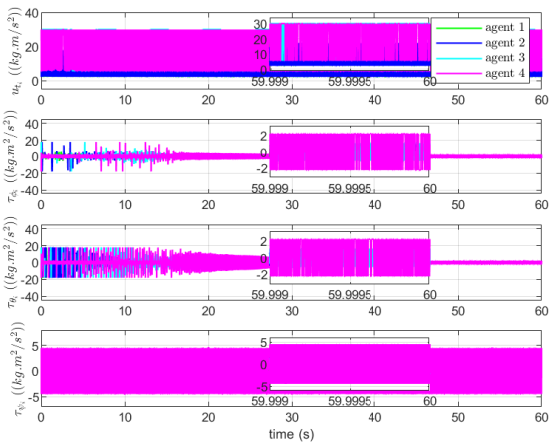

FIGURE 12: The profile of control inputs using conventional SMC with higher robust gains

[12] Tianpeng Huang, Deqing Huang, Zhikai Wang, and Awais Shah. Robust tracking control of a quadrotor uav based on adaptive sliding mode controller. Complexity, 2019.

[13] Imil Hamda Imran, Azhar M. Memon, Dilek Funda Kurtulus, Srikanth Goli, and Luai Muhammad Alhems. Extended sliding mode control scheme for a vtol uav with time-varying disturbances. In AIAA AVIATION 2023 Forum, page 4461, 2023.

[14] Imil Hamda Imran, Azhar M Memon, Dilek Funda Kurtulus, Srikanth Goli, and Luai Muhammad Alhems. Extended discrete-time quasi-sliding mode control for vtol uav in the presence of uncertain disturbances. IEEE Access, 2023.

[15] Jie Huang and Zhiyong Chen. A general framework for tackling the output regulation problem. IEEE Transactions on Automatic Control, 49(12):2203–2218, 2004.

[16] Frank L Lewis, Darren M Dawson, and Chaouki T Abdallah. Robot manipulator control: theory and practice. CRC Press, 2003.

[17] Ahmed Eltayeb, Mohd Fuaad Rahmat, Mohd Ariffanan Mohd Basri, and Magdi S Mahmoud. An improved design of integral sliding mode controller for chattering attenuation and trajectory tracking of the quadrotor uav. Arabian Journal for Science and Engineering, 45:6949–6961, 2020.

[18] Ahmed Eltayeb, Mohd Fua'ad Rahmat, Mohd Ariffanan Mohd Basri, MA Mohammed Eltoum, and Magdi Sadek Mahmoud. Integral adaptive sliding mode control for quadcopter uav under variable payload and disturbance. IEEE Access, 10:94754–94764, 2022.

[19] Kumpati S Narendra and Anuradha M Annaswamy. Stable adaptive systems. Prentice Hall: Englewood Cliffs. NJ, 1989.

[20] Alessandro Astolfi, Dimitrios Karagiannis, and Romeo Ortega. Nonlinear and adaptive control with applications, volume 187. Springer, 2008.

[21] Xun Gu, Bin Xian, and Jieqi Li. Model free adaptive control design for a tilt trirotor unmanned aerial vehicle with quaternion feedback: Theory and implementation. International Journal of Adaptive Control and Signal Processing, 36(1):122–137, 2022.

[22] Imil Hamda Imran, Kieran Wood, and Allahyar Montazeri. Adaptive control of unmanned aerial vehicles with varying payload and full parametric uncertainties. Electronics, 13(2):347, 2024.

[23] Qi Han, Zhitao Liu, Hongye Su, and Xiangbin Liu. Filter-based disturbance observer and adaptive control for euler–lagrange systems with application to a quadrotor uav. IEEE Transactions on Industrial Electronics, 70(8):8437–8445, 2022.

[24] Junan Wang, Bing Zhu, and Zewei Zheng. Robust adaptive control for a quadrotor uav with uncertain aerodynamic parameters. IEEE Transactions on Aerospace and Electronic Systems, 2023.

[25] Xi Chen and Zhiyong Chen. Robust perturbed output regulation and synchronization of nonlinear heterogeneous multiagents. IEEE Transactions on Cybernetics, 46(12):3111–3122, 2015.

[26] Lijun Zhu and Zhiyong Chen. Robust homogenization and consensus

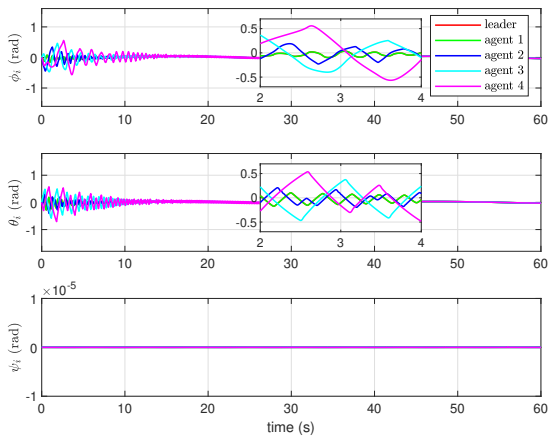

FIGURE 13: The profile of ϕ_i, θ_i and ψ_i using conventional SMC

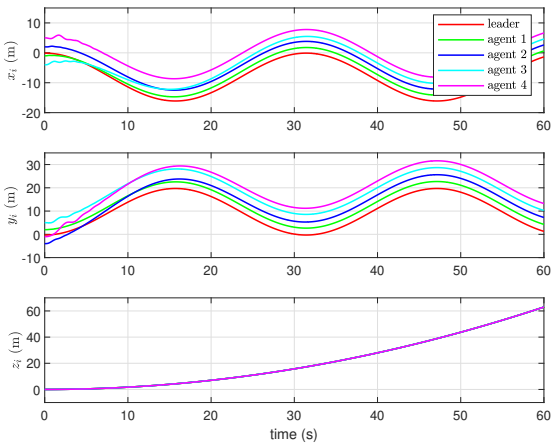

FIGURE 14: The profile of x_i, y_i and z_i using conventional SMC

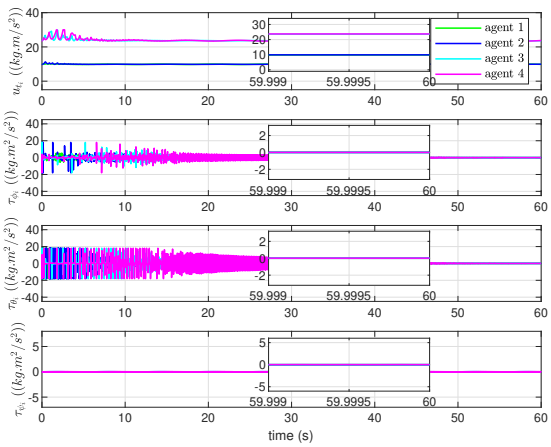

FIGURE 15: The profile of control inputs using proposed design with higher robust gains

of nonlinear multi-agent systems. Systems & Control Letters, 65:50–55, 2014.

[27] Frank L Lewis, Hongwei Zhang, Kristian Hengster-Movric, and Abhijit Das. Cooperative control of multi-agent systems: optimal and adaptive design approaches. Springer Science & Business Media, 2013.

[28] Imil Hamda Imran, Zhiyong Chen, Lijun Zhu, and Minyue Fu. A distributed adaptive scheme for multiagent systems. Asian Journal of Control, 24(1):46–57, 2022.

[29] Jimin Yu, Chuanyou Yan, and Mei Huang. Research of consistency problem for quadrotor uav system with leader-follower. In 2019 Chinese Automation Congress (CAC), pages 616–621. IEEE, 2019.

[30] Patrik Kolaric, Ci Chen, Ankur Dalal, and Frank L Lewis. Consensus controller for multi-uav navigation. Control Theory and Technology, 16:110–121, 2018.

[31] AnhDuc Dang and Joachim Horn. Formation control of leader-following uavs to track a moving target in a dynamic environment. Journal of Automation and Control Engineering Vol, 3(1), 2015.

[32] Ben Yun, Ben M Chen, Kai Yew Lum, and Tong H Lee. Design and implementation of a leader-follower cooperative control system for unmanned helicopters. Journal of Control Theory and Applications, 8:61–68, 2010.

[33] ZHOU Panpan et al. Semi-global leader-following consensus-based formation flight of unmanned aerial vehicles. Chinese Journal of Aeronautics, 35(1):31–43, 2022.

[34] Abdullah Basci. Robust consensus-based formation control of a group of uav. Elektronika ir Elektrotechnika, 29(4):4–10, 2023.

[35] Kheireddine Choutri, Mohand Lagha, and Laurent Dala. Distributed obstacles avoidance for uavs formation using consensus-based switching topology. International Journal of Computing and Digital Systems, 8(2):167–178, 2019.

[36] Tianlai Xu, Jinlong Liu, Zexu Zhang, Guodong Chen, Di Cui, and Huiping Li. Distributed mpc for trajectory tracking and formation control of multi-uavs with leader-follower structure. IEEE Access, 2023.

[37] Yongbin Sun, Jiayi Li, Zixuan Wang, Xiuyu He, Qiang Fu, and Yao Zou. Distributed formation-aggregation control algorithm for a cluster of quadrotors. Journal of the Franklin Institute, 360(3):1560–1581, 2023.

[38] Qiong Lin, Zhiqiang Miao, Yaonan Wang, Zheng-Guang Wu, Wei He, and Rafael Fierro. Differentiator-based bearing-only formation control of quadrotors. International Journal of Robust and Nonlinear Control, 33(17):10606–10624, 2023.

[39] Chang-E Ren and CL Philip Chen. Sliding mode leader-following consensus controllers for second-order non-linear multi-agent systems. IET Control Theory & Applications, 9(10):1544–1552, 2015.

[40] Zhen Zhou, Hongbin Wang, Yueling Wang, Xiaojun Xue, and Mingquan Zhang. Distributed formation control for multiple quadrotor uavs under markovian switching topologies with partially unknown transition rates. Journal of the Franklin Institute, 356(11):5706–5728, 2019.

[41] Haci Mehmet Guzey, Travis Dierks, Sarangapani Jagannathan, and Levent Acar. Modified consensus-based output feedback control of quadrotor uav formations using neural networks. Journal of Intelligent & Robotic Systems, 94:283–300, 2019.

[42] Haibo Du, Wenwu Zhu, Guanghui Wen, Zhisheng Duan, and Jinhu Lü. Distributed formation control of multiple quadrotor aircraft based on nonsmooth consensus algorithms. IEEE transactions on cybernetics, 49(1):342–353, 2017.

[43] AM Popov, DG Kostrygin, AA Shevchik, and B Andrievsky. Speed-gradient adaptive control for parametrically uncertain uavs in formation. electronics 2022, 11, 4187, 2022.

[44] Qiaoping Li, Yu Chen, and Kun Liang. Predefined-time formation control of the quadrotor-uav cluster'position system. Applied Mathematical Modelling, 116:45–64, 2023.

[45] Jie Lin, Yaonan Wang, Zhiqiang Miao, Qiong Lin, Guoqiang Hu, and Rafael Fierro. Robust linear-velocity-free formation tracking of multiple quadrotors with unknown disturbances. IEEE Transactions on Control of Network Systems, 2023.

[46] Anil Guclu. Designing autopilot and guidance algorithms to control translational and rotational dynamics of a fixed wing VTOL UAV. PhD thesis, Middle East Technical University, 2020.

[47] Imil Hamda Imran, Rustam Stolkin, and Allahyar Montazeri. Adaptive control of quadrotor unmanned aerial vehicle with time-varying uncertainties. IEEE Access, 2023.

IMIL HAMDA IMRAN received the B.S. degree in Electrical Engineering from Andalas University, Indonesia, in 2011, the M.S. degree in Systems and Control Engineering from King Fahd University of Petroleum and Minerals, Saudi Arabia, in 2015, and the Ph.D. degree in Electrical Engineering from The University of Newcastle, Australia, in 2020.

He was a Postdoctoral Research Associate at the Department of Engineering, Lancaster University, United Kingdom from 2020 to 2022. He is currently a Postdoctoral Fellow at the Applied Research Center for Metrology, Standards, and Testing, King Fahd University of Petroleum and Minerals, Saudi Arabia. His research interests include networked control systems, multi-agent systems, nonlinear control, and adaptive control.

DILEK FUNDA KURTULUS received the B.S. and the M.S. degrees in aerospace engineering from Middle East Technical University, Ankara, Turkey in 2000 and in 2002, respectively and the Ph.D. degree in aerospace engineering from ENSMA/Université de Poitiers, Poitiers, France.

In 2006, she was post-doctoral researcher in Laboratoire d'Etudes Aérodynamique, ENSMA Poitiers, France and in Laboratoire de Combustion et Systèmes Réactifs, CNRS, Orléans, France. Since 2018, she has been a Professor with Aerospace Engineering Department, Middle East Technical University, Ankara, Turkey. Her research interests include aircraft design, unsteady aerodynamics, unmanned air vehicles.

Dr. Kurtulus was a recipient of the Amelia Earhart Fellow from Zonta International in 2005, NATO Scientific Achievement Award in 2011, Turkish Academy of Science Young Scientific Award in 2012 and Zonta International Centennial Recognition Award of Turkey in 2019.

AZHAR M. MEMON was born in Pakistan in 1987. He received his B.E. degree in Electronics from the National University of Sciences and Technology (NUST), Pakistan, in 2009, M.Sc. from National University of Singapore (NUS), Singapore in Automation and Control Engineering, in 2010, and Ph.D. from King Fahd University of Petroleum and Minerals (KFUPM, Saudi Arabia, in 2015.

From 2009 to 2010, he was a Research Engineer with NUS and taught as a lecturer in NUST in 2011. After completing his Ph.D., he joined the R&D department of Rosen Group as a Sensors and Algorithm specialist. In 2019, he joined KFUPM as an Assistant Professor where he is actively participating in managing various client and internally funded research projects and teaching. He has published several peer-reviewed research articles and conference papers in reputable journals and international conferences. His research interests are diverse and include Control Systems, Signal Processing, Data analytics, Nondestructive Testing, and Aquaponics. Website: www.azharmemon.com

SRIKANTH GOLI was born in Hyderabad, India. He received Ph.D. in 2019 from the Aerospace Engineering Department, Indian Institute of Technology Kharagpur, India.

From 2019 to 2022, he carried out research at various Academic Institutions and Industries. He is currently pursuing Post-doctoral research at the Applied Research Center for Metrology, Standards, and Testing (ARCMST), King Fahd University of Petroleum and Minerals (KFUPM), Saudi Arabia. His research interests include aircraft design, experimental and numerical fluid dynamics, and unmanned air vehicles.

He has memberships in professional societies such as the National Society of Fluid Mechanics and Fluid Power, the Indian Society of Theoretical and Applied Mechanics, and the Aeronautical Society of India.

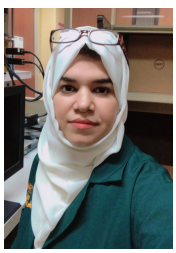

TAIBA KOUSER was born in Faisalabad, Pakistan. She earned the doctoral degree from the School of Aerospace Engineering at Huazhong University of Science and Technology, Wuhan, China in 2021. Currently, she is a Post-Doctoral Researcher with the Applied Research Center for Metrology, Standards, and Testing (ARC-MST), King Fahd University of Petroleum and minerals (KFUPM), Dhahran, Saudi Arabia. Her area of research is computational fluid dynamics. Her research interests include drag reduction, unsteady aerodynamics and aeroacoustics.

LUAI MUHAMMAD ALHEMS received the Ph.D. degree from Texas A & M University, College Station, TX, USA, in 2002. He is currently a Professor of thermo-fluid with the Mechanical Engineering Department, King Fahd University of Petroleum and Minerals (KFUPM), Dhahran, Saudi Arabia. He is the Director of the Applied Research Center for Metrology, Standards, and Testing (ARC-MST), Research Institute. Regional authorities have recognized him for his research work. He has published more than 180 journal papers and patents. His research interests include gas turbine, energy systems, failure analysis, wind energy, and energy conservation.